



Wet magmatic processes during the accretion of the deep crust of the Oman Ophiolite paleoridge: Phase diagrams and petrological records

DOI:

[10.1016/j.tecto.2021.229051](https://doi.org/10.1016/j.tecto.2021.229051)

Document Version

Accepted author manuscript

[Link to publication record in Manchester Research Explorer](#)

Citation for published version (APA):

Koepke, J., Feig, S. T., Berndt, J., & Neave, D. (2021). Wet magmatic processes during the accretion of the deep crust of the Oman Ophiolite paleoridge: Phase diagrams and petrological records. *Tectonophysics*, [229051]. <https://doi.org/10.1016/j.tecto.2021.229051>

Published in:

Tectonophysics

Citing this paper

Please note that where the full-text provided on Manchester Research Explorer is the Author Accepted Manuscript or Proof version this may differ from the final Published version. If citing, it is advised that you check and use the publisher's definitive version.

General rights

Copyright and moral rights for the publications made accessible in the Research Explorer are retained by the authors and/or other copyright owners and it is a condition of accessing publications that users recognise and abide by the legal requirements associated with these rights.

Takedown policy

If you believe that this document breaches copyright please refer to the University of Manchester's Takedown Procedures [<http://man.ac.uk/04Y6Bo>] or contact uml.scholarlycommunications@manchester.ac.uk providing relevant details, so we can investigate your claim.



1
2 **Wet magmatic processes during the accretion of the deep crust of the Oman**
3 **Ophiolite paleoridge: Phase diagrams and petrological records**

4
5 *Revised Version*
6
7

8 **J. Koepke^{1*}, S.T. Feig², J. Berndt³, D.A. Neave⁴, and the Oman Drilling Project Science**
9 **Team⁵**

10 ¹Institut für Mineralogie, Leibniz Universität Hannover, Callinstrasse 3, 30167 Hannover,
11 Germany

12 ²University of Tasmania, Hobart TAS 7001, Australia

13 ³University Muenster, Corrensstraße 24, 48149 Münster, Germany

14 ⁴Department of Earth and Environmental Sciences, The University of Manchester, Oxford Road,
15 Manchester, M13 9PL, UK

16 ⁵Since we present data in this manuscript from the Oman Drilling Project which are not officially
17 published in the related proceedings (<http://publications.iodp.org/other/Oman/OmanDP.html>) it
18 is necessary to include the OmanDP Science team as author.

19
20 Corresponding author: Jürgen Koepke (koepke@mineralogie.uni-hannover.de)
21

22 **Highlights:**

- 23 • Magmatic accretion of the deep crust of the Oman Ophiolite paleoridge was wet
24 • Water in Oman parental melts enables the formation of crustal wehrlites
25 • Phase diagrams for hydrous crust formation during subduction zone initiation
26 • Construction of phase diagrams for the axial melt lens at 50 MPa in a wet system
27 • importance of in-situ crystallization during the accretion of the Oman paleocrust

28

29 **Keywords:**

- 30 • Experimental study
- 31 • Hydrous MORB-systems
- 32 • Oman Drilling Project
- 33 • Oman ophiolite
- 34 • Fast-spreading oceanic crust
- 35 • Wehrlites

36 **Abstract**

37 The Oman Ophiolite is regarded as an analogue to modern fast-spreading ocean ridge systems in
38 an environment of subduction zone initiation. In contrast to recent mid-ocean ridge basalts from
39 the East Pacific Rise, parental melts at the Oman paleoridge are assumed to be hydrous in nature.
40 In order to constrain the role of water during magmatic accretion processes in the deep crust at
41 the Oman paleoridge, we evaluated several experimental studies in hydrous tholeiitic systems
42 performed at shallow pressures. We concluded that the wehrlitic phase assemblage (olivine
43 coexisting with clinopyroxene but without plagioclase) is the most significant feature indicative
44 of high prevailing water activities. The stability of the wehrlitic assemblage decreases with
45 decreasing pressure (not stable in the upper plutonic crust) and depends on the chemical system
46 (only stable in primitive MORB systems).

47 We applied these results to plutonic rocks from cores drilled as part of the Oman Drilling
48 Project (OmanDP). A key observation is the presence of coherent wehrlitic layers within the
49 layered gabbro series, which are frequent in the lowermost gabbros (20%), relative sparse in the
50 mid-crust (6%), and absent from the top of the plutonic crust at the dike/gabbro transition. Based
51 on the combined phase relations for hydrous MORB-type systems at shallow pressures, we
52 interpret this as a direct consequence of the presence of a significant water activity during the
53 accretion of the plutonic crust of the Oman paleoridge, and not as a local phenomenon related to
54 variations in temperature or bulk chemistry. These findings have implications for the mechanism
55 of accretion of the lower crust at the Oman paleoridge, supporting a model that significant parts
56 of the plutonic crust were produced by in-situ crystallization of primitive melt sills.

57

58 **1 Introduction**

59 The accretion and growth of oceanic crust at mid-ocean ridges generated by seafloor
60 spreading is one of the dominant processes in the chemical differentiation and physical evolution
61 of the Earth. Nearly 70% of the surface of our planet was built in this way. Oceanic crust from
62 fast-spreading ridge systems shows a relatively homogeneous, layered stratigraphy (e.g., Canales
63 et al., 2003). Here, the basic processes responsible for the generation of oceanic crust are ascent,
64 differentiation, and solidification of Mid Ocean Ridge Basalts (MORB), which are mainly
65 delivered from the axial melt lens (AML), sandwiched between the plutonic gabbroic layer and
66 the volcanic sheeted dike sequence. The melt lens, which is filled with nearly pure melt, is

67 underlain by crystal/melt mush that is in turn laterally surrounded by a transition zone of mostly
68 solidified material that grades into a completely crystalline zone of solidified gabbros (e.g., Vera
69 et al., 1990). The role of the AML during crustal accretion is still debated: either, this melt
70 reservoir is the source for the complete lower, gabbroic crust, formed by the suspension of
71 crystal mush formed here (the "gabbro glacier model", e.g., Henstock et al., 1993), or significant
72 parts of the plutonic crust originate from in situ crystallization in the deep crust (the "sheeted sill
73 model"; e.g., Kelemen et al., 1997). However, current consensus now favors "hybrid" models
74 that combine the two endmember models mentioned above (e.g., Mock et al., 2021b). The in-situ
75 crystallization in the lower crust is also supported from recent seismic experiments that indicate
76 the presence of deep melt sills under recent fast/intermediate-spreading ridges (see Carbotte et
77 al., 2021 and references herein). Since outcrops of the lower oceanic crust in modern fast-spread
78 crust are very rare and difficult to access, it is necessary to undertake corresponding studies on
79 ophiolites and on the Oman ophiolite in particular, which is regarded as the best example of fast-
80 spreading oceanic lithosphere thrust on land, and which has played a key role in establishing
81 fundamental principles in the geodynamics of mid-ocean ridges (e.g., Nicolas et al., 2000). The
82 Oman Ophiolite is also the target of the multi-national Oman Drilling Project (OmanDP,
83 <https://www.omandrilling.ac.uk/>) within ICDP (International Continental Scientific Drilling
84 Program) that addresses a diverse range of scientific questions relating to the formation,
85 hydrothermal alteration and weathering of oceanic lithosphere. Sections from drill cores obtained
86 within the OmanDP are the key samples used in this study.

87 In the present study we focus on the hydrous nature of the parental melts forming the
88 Oman ophiolite paleoridge, which is in contrast with the relatively dry nature of primary MORB
89 melts from the East Pacific Rise (EPR) that represents modern fast-spreading oceanic crust. We
90 first evaluate several experimental studies in wet tholeiitic systems performed at shallow crustal
91 pressures, in order to constrain the influence of water on the stabilities of the phases of the deep
92 crystal mush. Secondly, we apply the experimental results to gabbroic sequences from the
93 OmanDP drill cores, focusing on those features which can be regarded as resulting from the
94 hydrous nature of the parental melts. While the assessment that the parental melts at the Oman
95 paleoridge have been hydrous, is mainly based on the composition of the Oman lavas (MacLeod
96 et al., 2013), we focus in this paper on the plutonic foundation of the crust. We provide evidence
97 that characteristic phase relations recorded within the gabbroic crust could be interpreted as a
98 consequence of the presence of elevated water activities ($a_{\text{H}_2\text{O}}$) in the parental melts.

99

100 The Cretaceous Oman Ophiolite in the Sultanate of Oman shows complete and intact
101 sequences of fast-spreading oceanic crust in many locations. Basic descriptions of the ophiolite
102 and a geological map can be found in Nicolas et al. (2000). Zircon dating has revealed that the
103 paleocrust formed ~95 Ma ago under fast-spreading conditions with a half-spreading rate of 50 –
104 100 mm/yr (Rioux et al., 2012). In contrast with the contemporary fast-spreading mid-ocean
105 ridges such as the EPR, field relations and geochemical results suggest a polygenetic origin for
106 the Oman ophiolite (e.g., de Graaff et al., 2019). The first magmatic phase produced the so-
107 called V1 lavas and related gabbros that are very similar to the modern EPR, except that the
108 parental MORB melts show enhanced water contents due to the influence of the regional
109 subduction initiation (e.g., MacLeod et al., 2013). The lithologies formed by the phase-1
110 magmatism build the classical "Penrose" crust (Anonymous, 1972) consisting of, from the
111 bottom to the top, the Moho transition zone, layered gabbros, foliated gabbros, isotropic gabbros,
112 sheeted dikes and pillow basalts. A schematic section through this type of crust and images from
113 outcrops from rocks formed by phase-1 magmatism are shown in Fig. 1 and 2 a-d, respectively.
114 The parental melts for the phase-1 magmatism are of MORB-type, the so called "Geotimes"
115 basalts (e.g., Godard et al., 2003), but with trace element characteristics similar to Eocene forearc
116 basalts (FAB) from the Izu-Bonin-Mariana (IBM) islands (MacLeod et al., 2013), and are thus
117 interpreted as typical basalts generated by decompression peridotite melting during the initiation
118 of an intraoceanic subduction zone (e.g., Agard et al., 2020). By applying MELTS modeling
119 (Ghiorso and Sack, 1995) to the Oman "Geotimes" lava distributed all over the ophiolite,
120 MacLeod et al. (2013) estimated initial water contents in the range 0.2 to > 1 wt% H₂O, which
121 are significantly higher than modern EPR MORB (~0.2 wt% H₂O, le Roux et al., 2006). MELTS
122 calculations related to varitextured gabbros from the southernmost part of the ophiolite generated
123 during accretion phase 1 reveal water contents of 0.4 to 0.8 wt% (Müller et al., 2017).

124 A second magmatic phase based on flux-induced peridotite melting, normally intruding
125 into the rocks of the first magmatic phase, formed characteristic lithologies like andesitic and
126 boninitic basalts, as well as clinopyroxene-phyric lavas (V2 basalts: see Godard et al. 2003) in
127 the volcanic crust. The corresponding rocks in the plutonic crust, often named "late-stage
128 intrusives" (e.g., Lippard et al., 1986) are wehrlites, gabbronorites, and felsic intrusions (so-
129 called plagiogranites). A schematic section through this type of crust is shown in Fig. 1, and
130 images from outcrops from rocks formed by phase-2 magmatism are shown in Fig. 2 e-h. Such

131 lithologies are unknown from recent fast- and intermediate spreading systems, underlining the
132 difficulties faced when comparing the Oman ophiolite with modern EPR crust. The two-stage
133 magmatic origin of the Oman ophiolite is in accord with models on subduction zone initiation
134 (e.g., Stern, 2004), with an initial phase of spreading in a forearc regime producing typical FAB
135 basalts by decompression mantle melting comparable with the Oman Geotimes basalts
136 (MacLeod et al., 2013), and a second magmatic phase characterized by flux mantle melting.
137 Concerning the tectonic setting of the Oman ophiolite most scientists favor a model on
138 subduction zone initiation (e.g., MacLeod et al., 2013, Rioux et al., 2013; Agard et al., 2020).
139 The strongest arguments for this are the recorded ages in the metamorphic sole (Guilmette et al.,
140 2018) and the high pressures estimated for its formation (up to 1.3 GPa, Cowan et al., 2014).

141 In spite of the inferred subduction initiation setting of the Oman ophiolite, the following
142 observations related to the first magmatic phase nevertheless demonstrate a close similarity with
143 the modern, fast-spreading EPR: (1) a continuous layered crustal structure with a typical crustal
144 thickness of ~ 6 km, including a coherent plutonic section consisting of typical layered gabbros
145 with a layering parallel to the crust/mantle boundary; (2) the absence of amagmatic spreading
146 that is common at slow-spreading ridges; (3) a very narrow range of zircon crystallization ages
147 across the width of the ophiolite (max ~100 km) sampled normal to the ridge direction; (4) spinel
148 compositions that overlap with those for peridotites from modern ridges (Python et al., 2008);
149 and (5) a well-developed sheeted dike sequence, orientated perpendicular to the Moho.

150
151 Many experimental studies conducted in tholeiitic systems under dry conditions in order to
152 understand the evolution of MORB (see reviews in Elthon, 1991, and Grove et al., 1992). These
153 studies are extremely helpful for evaluating details of crystallization processes in dry MORBs,
154 such as those from the modern EPR, but they fail to predict phase relations and phase
155 compositions in hydrous MORB melts, like those "Geotimes" basalts
156 with FAB characteristics forming the main part of the basalts accreted at the Oman paleo ridge.
157 For this, experimental studies in hydrous systems performed under shallow pressures are
158 necessary.

159 The main effect of water in basaltic systems is the delay in plagioclase in favor of
160 clinopyroxene saturation (e.g., Feig et al., 2006; Gaetani et al., 1993; Neave et al., 2019), with a
161 dramatic effect both on phase relations and phase compositions. The presence of water may
162 stabilize the paragenesis of olivine and clinopyroxene without plagioclase, thus producing a

163 wehrlitic crystallizing assemblage (Feig et al., 2006; Koepke et al., 2009) with the potential to
164 form wehrlites, if these crystals accumulate and segregate. A further effect of suppressing
165 plagioclase crystallization is that the melts get enriched in plagioclase component resulting in
166 melts in which Al_2O_3 is significantly enhanced, which is well known from calc-alkaline basaltic
167 series typically for subduction-zone environments (i.e. High Alumina basalts, Kuno, 1960;
168 Crawford et al., 1987). Another effect of water in basaltic melts is that the liquidus and
169 temperatures of mineral saturations are lowered (e.g., Almeev et al., 2007; Danyushevsky, 2001),
170 and that crystallizing plagioclases are strongly enriched in anorthite content compared to dry
171 conditions (e.g., Botcharnikov et al., 2008; Sisson and Grove, 1993).

172 Considering the differentiation of MORB within oceanic magma chambers, likely
173 pressures of crystallization can be evaluated quite precisely. Pressures around ~ 200 MPa can be
174 expected for the crystallization processes at the bottom of the crust, corresponding to ~ 6 km
175 depth below sea floor. Lowest pressures of ~ 50 MPa can be expected for crystallization
176 processes within the AML, which is sandwiched between the gabbro and the sheeted dike
177 sequence at about 1.5 km below the seafloor. In dry systems, such a pressure range would have
178 only a small effect on phase relations. However, this is not the case in hydrous systems because
179 water activity strongly depends on water solubility, which varies significantly with pressure,
180 especially at pressures less than 500 MPa (Berndt et al., 2002).

181 Experiments performed at both dry and at hydrous conditions show that the basic process
182 responsible for the generation of oceanic crust is fractional crystallization of a MORB-type
183 parental melt formed by decompression melting in the shallow mantle beneath the ridge at 1 to 2
184 GPa (see review in Elthon, 1991). The main stage of crust accretion is manifested by cotectic
185 crystallization in MORB magmas with the characteristic phase assemblage olivine–plagioclase–
186 clinopyroxene which, after accumulation, form mushes that produce typical olivine gabbros.
187 Berndt et al. (2005), Feig et al. (2006; 2010), and Koepke et al. (2018) systematically
188 investigated experimental phase equilibria in primitive and evolved MORB-type basaltic systems
189 as a function of oxygen fugacity ($f\text{O}_2$) and $a\text{H}_2\text{O}$. Their combined experimental data enable a
190 profound insight into the main and late stage of crystallization processes within magma
191 chambers at mid-ocean ridges. It is our attempt to integrate the results of these studies, which are
192 perfect suited for highlighting the role of water during crystallization/differentiation, with field
193 and petrographic observations related to the Oman phase-1 gabbros, in order to get new insight
194 into the role of water during the magmatic accretion at the Oman paleoridge. All of these

195 experimental studies used a very similar methodical approach and have been performed by the
196 same working group in the same, highly specialized high-pressure facility. Thus they are well-
197 suited for a global discussion on the relations and stabilities of the phases in MORBs from
198 spreading systems in which elevated water activities play a significant role.

199

200 **2 Materials and Methods**

201 *2.1 Experimental studies used*

202 In this paper we use results from Berndt et al. (2005), Feig et al. (2006; 2010), and
203 Koepke et al. (2018), which were performed at shallow crustal pressures in different hydrous
204 MORB-type systems, in order to evaluate phase relations applicable to magmatic accretion of the
205 deep crust at the Oman paleoridge. These studies report crystallization experiments with glassy
206 starting materials that were performed in the same internally heated pressure vessel (IHPV) at the
207 University of Hannover. Details of the experimental approaches and the starting materials used,
208 pressures and temperatures applied, prevailing water activities and redox conditions can be
209 obtained from Table 1 and from the individual papers. The apparatus used, a vertically oriented
210 IHPV pressured with Ar as pressure medium, is described in detail in Berndt et al. (2002). Under
211 intrinsic conditions (pure Ar) this equipment is fairly oxidizing with fO_2 varying between
212 QFM+3.2 and QFM+4.2 (QFM corresponds to the quartz-magnetite-fayalite oxygen buffer)
213 under water-saturated conditions. In order to perform experiments at more reducing conditions,
214 Ar-H₂ gas mixtures were used as the pressure medium to attain the required fH_2 . The fH_2
215 prevailing in the IHPV at high P and T was monitored with a Shaw-membrane made of platinum
216 (Berndt et al., 2002). The fH_2 applied in the experiments considered here maintained redox
217 conditions corresponding to fO_2 values between QFM and QFM+2 under water-saturated
218 conditions. Within the sample capsule, fH_2 was fixed due to the inward diffusion of hydrogen
219 controlling the fO_2 inside the capsule through the equilibrium reaction of water formation ($H_2 +$
220 $1/2 O_2 \leftrightarrow H_2O$). Thus, in the capsules with $a_{H_2O} < 1$, the redox conditions were more reducing
221 than in the experiments with $a_{H_2O} = 1$ (for details see Botcharnikov et al., 2005). Since a_{H_2O}
222 was varied between < 0.1 and 1 (Table 1), the overall variation in fO_2 in all experimental series
223 was in the range between \sim QFM-3 and \sim QFM+4.2, thus covering the range of oxygen
224 fugacities prevailing in natural MORB magmas (Bézos and Humler, 2005; Zhang et al., 2018;
225 O'Neill et al., 2018).

226 *2.2 Samples from the ICDP OmanDP*

227 The phase relations obtained from experimental studies described above have been
228 applied to rocks drilled within the ICDP OmanDP to address the influence of a water activity on
229 phase-1 magmatic processes operating during the accretion of the deep crust at the Oman
230 paleoridge in an environment of subduction zone initiation. For this, we used samples with
231 characteristic phase parageneses thought to represent a record of hydrous processes. We used
232 samples of drill cores penetrating crustal series from five sites: CM1 and CM2 – traverses
233 through the crust/mantle transition; GT1 – a traverse through the layered gabbro (deep gabbro
234 traverse); GT2 – a traverse through the transition between the layered and foliated gabbro
235 (shallow gabbro traverse); GT3 – a traverse through the gabbro/dike transition. The absolute
236 heights of the CM drill sites within a crustal profile can be obtained directly from the cores (in
237 meters above mantle harzburgite): CM1 - 300 m; CM2 - 130 m. For the GT1 and GT2 cores, the
238 absolute crustal heights of the sites can be obtained from site surveys performed before the
239 drillings: GT1 ~ 1170 m; GT2 ~ 2700 m (see OmanDP, <https://www.omandrilling.ac.uk/>). The
240 crustal height of site GT3 can be estimated as ~ 4500m, corresponding to an average from
241 Nicolas and Boudier (2000).

242 These sites are located in the Southernmost massifs of the Oman ophiolite, where the
243 influence of the phase-2 magmatism is low. All these drill sites have been carefully selected by
244 the multi-national working groups within the frame of the OmanDP to ensure that crosscutting
245 lithologies from the phase-2 magmatism don't play any role. This attempt was confirmed during
246 the phase of detailed core characterization, which was performed on the Japanese drill ship
247 Chikyu. Background information, details on the aims of the project, documented in the original
248 ICDP proposal, as well as information of the operational part can be found on the OmanDP
249 home page <https://www.omandrilling.ac.uk/>. Core characterization followed the methodical
250 guidelines of IODP (International Ocean Discovery Program), and, due to close cooperation with
251 IODP, the scientific results of the OmanDP obtained so far are published under the umbrella of
252 the IODP publishing platform (Kelemen et al., 2020).

253

254 **3 Results**

255 *3.1 Phase diagrams for hydrous magmatism within the oceanic crust*

256 The best approach to evaluate phase relations in hydrous MORB-type system to
257 investigate crystallization processes related to phase-1 magmatism in the axial magma chambers
258 of the Oman paleoridge is to use phase diagrams based on experiments in corresponding hydrous
259 systems performed at shallow crustal pressures. For this, we used four experimental phase
260 equilibria studies initiated to investigate relations and compositions of minerals and melts in
261 MORB systems (Berndt et al., 2005; Feig et al., 2006, 2010; Koepke et al., 2018). Fig. 3 shows
262 the combined results of these studies, where the upper three diagrams address variations in the
263 chemical system performed at identical pressure (200 MPa), while the lower panels focus on the
264 effect of pressure (100, 200, and 500 MPa) in a single chemical system.

265 Fig. 3a shows phase relations in a primitive natural MORB system from Feig et al.
266 (2010), derived from a re-melted microgabbro from the IODP (International Ocean Drilling
267 Program) Hole 735B drilled at the Southwest Indian Ridge. Fig. 3b presents experiments
268 performed with an average MORB composition from Berndt et al. (2005) obtained from the data
269 base PetDB, synthesized from oxides. Fig. 3c is based on experiments performed in a late-stage
270 MORB system from Koepke et al. (2018), derived with a statistical approach using evolved fresh
271 MORB glasses from the database PETDB highest in FeO and TiO₂ ("FeTi basalt"), which are
272 assumed to represent the last frozen liquids erupted at the seafloor generated by extensive
273 differentiation of MORB. This composition includes P₂O₅ (and sulfur in some experiments). Fig.
274 3d-f present phase relations from Feig et al. (2006), who used the same system as that from Feig
275 et al. (2010), but applied different pressures (100, 200, 500 MPa) under more oxidizing
276 conditions. The compositions of the systems used are presented in Table 1.

277 Due to the buffering of $f\text{H}_2$ in the experiments, $f\text{O}_2$ varies in a given experimental series
278 by about three orders of magnitude, depending on the prevailing water activity in the individual
279 runs (see section 2.1). This is demonstrated in the experiments shown in Fig. 3d-f, by the dotted
280 vertical lines, where $f\text{O}_2$ varies between QFM+1 for the runs with lowest water activity, and
281 QFM+4.2 for the runs at water saturation. A similar range in $f\text{O}_2$ is given for the diagrams in Fig.
282 3a-c, where this effect is not explicitly included in the diagrams. Since basalts from forearcs are
283 more oxidized than basalts from normal ridges (see review in Cottrell et al., 2021 in press), we
284 present in Fig. 3a-c phase diagrams from experiments that were performed under elevated

285 oxygen fugacities at values for $QFM > 1$ at water saturation, except for Fig. 3b, where the
286 corresponding experiments were performed close to the QFM buffer.

287 With the help of the combined phase diagrams shown in Fig. 3, we are able to constrain
288 phase relations in hydrous systems within the axial magma chambers beneath ocean spreading
289 centers. Key observations are the crossing saturation curves for plagioclase and clinopyroxene
290 with increasing water content, shown in Fig. 3a, e, f. These phase relations predict a near
291 liquidus phase assemblage of only olivine and clinopyroxene, if a relatively high amount of
292 water is present in the melt. If these crystals segregate and accumulate, wehrlitic mushes could
293 be produced, from which crustal wehrlites would form following the extraction of residual melts
294 (yellow fields in Fig. 3). Thus, the presence of wehrlites instead of troctolites as early cumulates
295 is strongly indicative of a hydrous magmatic environment. The combined phase diagrams
296 highlight further features related to the potential of the system to produce wehrlites. Specifically,
297 the effect depends strongly on the chemical system and the pressure; the wehrlite assemblage is
298 only stable in the most primitive system, (primitive MORB-type system, Table 1), and the
299 potential for forming the wehrlite assemblage decreases with pressure. In the primitive MORB
300 system considered, the wehrlite field shrinks considerably from 500 to 200 MP (Fig. 3e and f)
301 and disappears entirely at 100 MPa (Fig. 3d). We discuss aspects on wehrlite formation further in
302 section 4.1, highlighting phase relations observed in Oman magmatic phase-1 gabbros.

303 Although the phase diagram compilation in Fig. 3 is designed for hydrous magmatic
304 processes that operated during the accretion of the Oman paleocrust, we note that they can also
305 generally be applied to MORB-type basalts of similar shallow spreading settings. The Oman
306 ophiolite stands for a typical example of fore-arc spreading environment, and we expect to see
307 similar features in other ophiolites with similar geotectonic setting or in fore-arc systems of the
308 actual oceans (i.e., the archetypal Izu-Bonin-Mariana intra-oceanic arc, Arculus et al., 2019).

309 *3.2 Phase diagrams for melts residing in the AML of fast-spreading mid-ocean ridges*

310 At fast- (and intermediate-) spreading ridges, the AML, sandwiched between the gabbro
311 and sheeted dike sequences at about 1.5 km below the seafloor, corresponding to a lithostatic
312 pressure of 50 MPa, are regarded as key reservoirs where crystallization/differentiation takes
313 place (e.g., Coogan, 2014; Wanless and Shaw, 2012). Interestingly, in spite of the importance of
314 these melt reservoirs that are responsible for the accretion of large parts of the Earth's crust, no
315 phase diagrams exist for MORB-type systems at a pressure of 50 MPa. Of course, 1 atm

316 experiments can be used for completely dry systems (e.g., Tormey et al., 1987), since the
317 pressure dependence of phase relations in dry systems is insignificant, at least over the low
318 pressure range considered here. However, this is not the case for hydrous systems, since water
319 activity, which has a significant influence on phase relations and phase composition, varies
320 considerably with pressure due to the strong dependence of water solubility in silicate melts on
321 pressure (Berndt et al., 2002). In Fig. 4, we present two phase diagrams constructed for a
322 hydrous MORB-type system at 50 MPa derived from Feig et al. 2006 and Koepke et al 2018,
323 suitable for predicting phase relations in the AML from fast-spreading mid-ocean ridge systems.

324 Fig. 4a shows the phase relations in a primitive natural MORB corresponding to an early
325 stage of differentiation from Feig et al. (2006), who studied the role of water and oxygen
326 fugacity on the phase equilibria and differentiation. Under oxidizing conditions, these authors
327 also studied the pressure dependence (100, 200, and 500 MPa), which enable us to construct a
328 phase diagram for 50 MPa by extrapolating Fig. 4 of Feig et al. (2006), where the saturation
329 temperatures of the occurring mineral phases as a function of pressure under water-saturated
330 conditions are shown. Since the pressure influence was only investigated at relatively high
331 oxygen fugacities, the redox conditions for the 50 MPa phase diagram are also relatively
332 oxidizing, ranging from QFM+1 for less hydrous conditions to QFM+4.2 at water-saturation.
333 Feig et al. (2006) showed that common petrological models for evaluating differentiation trends
334 in MORB like MELTS (Ghiorso and Sack, 1995) and COMAGMAT (Ariskin, 1999) failed to
335 predict the experimental phase relations under hydrous conditions at shallow crustal pressures.
336 Therefore, the extrapolation of experimental results to 50 MPa is the best available way to
337 estimate reliable trends of magma evolution in a primitive hydrous tholeiitic system at the
338 magmatic conditions prevailing in the AML of mid-oceanic ridges.

339 Fig. 4b shows the phase relations at 50 MPa for a typical MORB late-stage system, which
340 was investigated by Koepke et al. (2018) at a pressure of 200 MPa. This system corresponds to a
341 highly evolved MORB, where FeO and TiO₂ are strongly enriched due to extended
342 differentiation under reducing conditions before Fe-Ti oxide saturation is reached. Such
343 compositions are well-known from glasses erupted at the seafloor (Fe-Ti basalts), implying that
344 such evolved melts exist within some AMLs. The pressure dependence of the mineral saturation
345 temperatures at water-saturation was taken from Feig et al. (2006; see above) to construct this
346 diagram.

347 *3.3 Petrographic records of hydrous magmatism within the lower crust*

348 The presence of wehrlitic assemblages within the phase-1 plutonics is a key indicator of
349 hydrous magmatic processes in MORB-type systems. Wehrlites are indeed observed within all
350 OmanDP cores penetrating the lower crust (CM1, CM2, GT1, GT2), but not in the core
351 through the dike/gabbro transition (GT3). Fig. 5 shows images from cores drilled through the
352 lower crust, showing wehrlitic layers alternating with olivine gabbros or olivine-bearing gabbros
353 within the layered series. Careful macroscopic and microscopic observations of the relevant
354 sections revealed that most of these layers are fully coherent with foliations in the gabbros of the
355 layered series (Kelemen et al., 2020), and are thus clearly not of crosscutting character, as is the
356 case for the magmatic phase-2 wehrlites – typically meter- to decimeter-thick bodies that intrude
357 into the layered series. Massive wehrlites with a maximal thicknesses of ~ 3 meter only occur in
358 the Moho transition zone drilled by CM1 and CM2, while true wehrlite layers in the GT1 and
359 GT2 cores only occur in the cm-scale (see on-site core descriptions for cores GT1 and GT2
360 available as electronic supplement in Kelemen et al., 2020). From the detailed characterization of
361 the CM cores it is a clear that all wehrlites are associated with the gabbroic series, and never with
362 the mantle sequence, indicating that these wehrlites are of crustal origin.

363 Thin sections of wehrlites in the four cores reveal different textures as shown in Fig. 6.
364 Pure wehrlites consisting exclusively of olivine and clinopyroxene (plus Cr-spinel) are typical
365 for the crust/mantle cores CM1 and CM2 (Fig. 6a, b). Here, wehrlites occur with poikilitic
366 clinopyroxene bearing small olivine chadacrysts (Fig. 6a), evidencing the crystallization order
367 olivine before clinopyroxene. In the gabbro cores GT1 and GT2 wehrlites occur in coherent,
368 maximally cm-thick layers with interstitial plagioclases (Fig. 6c), implying co-crystallization of
369 olivine and clinopyroxene before plagioclase. Thin sections showing contacts between gabbro
370 and wehrlitic layers reveal smooth, sutured contacts without discontinuities (Fig. 6d).
371 Macroscopic characterization of these contacts reveal planar interfaces that are characterized as
372 modally gradational or sharp and planar (Kelemen et al., 2020). Since many of these wehrlitic
373 rocks in the GT1 and GT2 cores bear more than 5 % plagioclase in the mode, the requirement for
374 naming such lithologies as "wehrlite" is not fulfilled (rock of olivine + clinopyroxene with
375 plagioclase < 5 mode%). Therefore, the scientific teams that described the cores on the Chikyu
376 named these rocks olivine melagabbro (Kelemen et al., 2020). However, in 97% of the
377 characterized intervals of melagabbro in core GT1, and 91% in GT2, the amount of
378 clinopyroxene is significantly higher than that of plagioclase, such that these gabbros clearly

379 show a wehrlitic character. Nevertheless, such wehrlitic gabbros, bearing prismatic olivine and
380 clinopyroxene and interstitial plagioclase, can also be regarded as indicators for hydrous
381 differentiation, since the order of crystallization obtained from the texture (olivine crystallized
382 together with clinopyroxene before plagioclase, Fig. 6c) clearly requires a relatively high
383 prevailing water activities during crystallization. It should be noted that true wehrlites are also
384 present in the crustal cores GT1 and GT2, as demonstrated by Fig. 6d. although not explicitly
385 noted in the corresponding proceedings (Kelemen et al., 2020).

386 A noteworthy occurrence of wehrlite was observed in the CM1 core, as demonstrated in
387 Fig. 7. Here, within a several decimeter-long core section, a dunite host rock bears both clusters
388 of wehrlitic (only olivine and clinopyroxene) and troctolitic (only olivine and plagioclase)
389 parageneses. This case is discussed in detail in the section 4.2.

390 Within the GT3 core penetrating the dike/gabbro transition, neither wehrlites nor
391 wehrlitic assemblages have been recorded during core description (Kelemen et al., 2020). Here,
392 an elevated prevailing water activity is expressed by the presence of magmatic amphibole in
393 most gabbros, especially in the so-called varitextured gabbros, which are characterized by the
394 presence of irregular domains/patches with significant variations in grain size, texture, and
395 mineral mode (for details on this term see MacLeod and Yaouancq, 2000). A typical example of
396 a varitextured gabbro from the GT3 core is presented in Fig. 8., where a granular textural domain
397 with magmatic amphibole enclosing plagioclase crystals is shown. In the poikilitic domains of
398 varitextured gabbros, plagioclase forms chadacrysts within poikilitic clinopyroxene,
399 demonstrating the crystallization order plagioclase before clinopyroxene. Later, interstitial
400 amphibole and Fe-Ti oxide crystallized in the granular domains in the interstices between the
401 poikilitic domains. The skeletal structure of clinopyroxene and the needle-like structure of
402 plagioclase often displaying skeletal morphology imply rapid growth (e.g., Holness, 2014), as it
403 is often observed in gabbros regarded to present the frozen filling of an AML (e.g., from EPR at
404 IODP Site 1256, Koepke et al., 2011; Koepke and Zhang, 2021). We discuss the phase relations
405 observed in these rocks considering the phase diagrams extrapolated for the prevailing pressure
406 of 50 MPa in section 4.5.

407

408 **4 Discussion**409 *4.1 Evidence for wet differentiation of gabbroic rocks from the OmanDP drill cores: formation*
410 *of wehrlites*

411 Wehrlites are often interpreted as records of melt accumulation or as products of
412 melt/peridotite interaction in the deeper lithospheric mantle at pressures below plagioclase
413 stability. Such rocks have been reported from the sub-continent mantle (e.g., Beard et al., 2007;
414 Shaw et al., 2005), in mantle from convergent margins (e.g., Parkinson et al., 2003; Peslier et al.,
415 2002), and from the sub-ocean mantle (Arai and Takemoto, 2007). These wehrlites often have
416 textures and fabrics typical of mantle rocks (e.g., porphyroclastic or protogranular textures), and
417 show the depleted phase compositions typical for mantle minerals (i.e., high Mg# in olivine and
418 clinopyroxene, very low TiO₂ in spinels). The formation of such "deep" wehrlite has also been
419 confirmed experimentally by reactive crystallization experiments involving lherzolite and
420 basaltic melts at typical mantle pressures (1 to 0.7 GPa) under nominally anhydrous conditions
421 (Saper and Liang, 2014). Since these wehrlites are restricted to a formation with mantle
422 involvement, such a genesis cannot be considered as model of formation of the crustal wehrlites
423 within the Oman ophiolite. For such rocks located at the crust/mantle boundary, Koga et al.
424 (2001) reported a trace element equilibrium with MORB-like liquids, thus disproving a model
425 that the crustal wehrlites are cumulates from an unusual parental melt. Based on an experimental
426 study, Koepke et al. (2009) concluded for discordant crustal wehrlites of the Wadi Haymiliyah in
427 (Haylan massif), which have been formed during magmatic phase 2 at the Oman paleo ridge, an
428 origin due to an advanced amount of water in a MORB system, enabling the suppression of
429 plagioclase crystallization.

430 For the wehrlites from the OmanDP drill cores investigated in this study, we suggest a
431 model of early crystallization and accumulation of olivine and clinopyroxene under a high water
432 activity within axial magma chambers of the Oman paleoridge (see section 3.1). In summary,
433 arguments for this are: (1) wehrlites form coherent layers within the layered gabbro series; (2)
434 olivine and clinopyroxene at least from one investigated wehrlite sample, show Mg#
435 significantly lower as those expected for mantle involvement (see section 4.2); (3) the poikilitic
436 structure of some clinopyroxene in wehrlites imply crystallization from a melt and not reaction
437 between mantle and MORB melts (Fig. 6a); (4) the observed wehrlitic assemblages are in fully
438 accordance with predictions from phase relations in hydrous MORB-type systems (see section

439 3.1); (5) textures of wehrlites are identical to those of the layered gabbros in terms of mineral
440 structures and foliation, and mantle textures are absent. The driving force for this is the well-
441 known feature that water suppresses plagioclase stability in favor of clinopyroxene, thus
442 expanding the "wehrlite field" to higher water activities in the phase diagrams of Fig. 3. For a
443 better understanding, we present a part of the phase diagram of Fig. 3e from Feig et al. (2006) in
444 Fig. 9, which focuses on main-stage crystallization where olivine, plagioclase and clinopyroxene
445 are considered, and other phases are ignored. The lithologies described in Fig. 9 correspond to
446 cumulate rocks which could be formed by accumulation of the crystal phases stable in each field
447 of the diagram.

448 Path #1 in Fig. 9 points to an evolution by "dry" differentiation, as typical for MORBs
449 from modern EPR. Under dry conditions, it is predicted that the first crystal mush to be formed
450 from two silicate phases is troctolitic, in agreement with predictions from (dry) 1-atm
451 experiments. Indeed, troctolites are well-known from the deep gabbro cores drilled by IODP
452 Expedition 345 at Hess Deep at EPR, where several decameter-thick sections of layered
453 troctolites have been recovered (Gillis et al., 2014). IODP Expedition 345 drilled 16 different
454 holes into the deep gabbros of Hess Deep, but none of them recovered wehrlites or a wehrlitic
455 gabbro. It should be also noted that troctolites are also very common in the lowermost Oman
456 gabbros, especially from the crust/mantle boundary. Since these are regarded to be derived from
457 hydrous melts in an environment of subduction zone initiation, this seems contradictory on a first
458 view. But, this is not the case, as we will see below. Path #2 in Fig. 9 shows a potential
459 differentiation path under high water activities, leading to the formation of wehrlitic mushes,
460 which may evolve into coherent layers of cumulate wehrlite typical for the lowermost crust
461 formed at the Oman paleoridge. Special differentiation conditions are indicated by path #3 in
462 Fig. 9, touching both the troctolite and wehrlite fields, which explains a peculiar phase situation
463 discussed in section 4.2 and shown in Fig. 7, where both wehrlitic and troctolitic domains coexist
464 within one thin section.

465 Fig. 9 shows that typical olivine gabbros, which are by far the most common rocks in the
466 gabbro series of the Oman lower crust, followed a differentiation path between paths #1 and #3,
467 resulting in the following succession: dunite – troctolite – olivine gabbros. It should be noted that
468 for these gabbro types it is not possible to predict from the phase diagram in Fig. 3a alone,
469 whether differentiation processes took place under dry conditions (like EPR gabbros) or with an
470 elevated water activity (environment of subduction zone initiation). However, for this, the

471 plagioclase composition can be used, as we discuss in the section 4.2 and more detailed in
472 section 4.4.

473 Many of the wehrlitic rocks from the OmanDP cores GT1 and GT2 bear late plagioclase
474 ("melagabbros", see section 3.3 and Fig. 6c), clearly indicating that crystallization/differentiation
475 did not end in the wehrlite field of Fig. 9, but continued with the saturation of plagioclase.

476 Considering Fig. 9, this can occur in two ways:

477 (1) The system simply continues cooling and oversteps the plagioclase saturation curve,
478 following path #2 to the end of the blue arrow in Fig. 9, enabling the crystallization of
479 plagioclase and leading to the evolution of plagioclase-bearing wehrlites. For these
480 "melagabbros" one would predict more evolved mineral compositions, since they correspond to a
481 more advanced differentiation state. However, due to the high water activity in these systems, the
482 plagioclases are extreme An-rich, with An contents very similar as in the earlier crystallized
483 wehrlites (see compositions in Feig et al., 2006). Moreover, since the high water activities also
484 cause higher oxygen fugacities, the systems evolves to higher $\text{Fe}_2\text{O}_3/\text{FeO}$ (Botcharnikov et al.,
485 2005), which drives the systems to high Mg# of olivine and clinopyroxene (Feig et al. 2006,
486 Berndt et al., 2005). The more the melt differentiates and moves away from the wehrlite field,
487 the more plagioclase is produced. This in turn favors the production of olivine gabbros, which
488 are effectively impossible to distinguish from olivine gabbros formed under drier conditions in
489 the field or under the microscope.

490 (2) Alternatively the system behaves isothermally but the water activity decreases (a
491 horizontal path from the wehrlite field to the left in Fig. 9). In this scenario the water activity
492 may be lowered by magma recharge and replenishment processes analogous to those responsible
493 for the creation of geochemically variable melt inclusion suites in diverse oceanic settings (e.g.,
494 MacLennan, 2008), enabling water-poor melts to mix with those water-enhanced residual melts
495 associated with the wehrlitic assemblage. The consequence of this is that the bulk water activity
496 is lowered, enabling the precipitation of plagioclase in a previously wehrlitic assemblage.

497 It should be noted that beside the water activity other factors like pressure and chemical
498 composition of the system are also important, whether the wehrlitic phase assemblage is stable or
499 not (see section 3.1). Further factors influencing wehrlite stability are variations in redox
500 conditions, and disequilibrium processes (e.g., melt/rock interaction, magma mixing), which are
501 not reflected in the phase diagrams of Fig. 3, since the corresponding experiments were
502 performed under equilibrium conditions.

503

504 *4.2 Wehrlitic and troctolitic parageneses within the same thin section*

505 One section of the gabbroic part of the OmanDP drill core CM1, which represents a
506 transect through the crust/mantle boundary, records a key phase relationship that affords
507 interesting perspectives on the formation of early cumulates, i.e. wehrlites and troctolites (Fig.
508 7). In spite of these rocks being very strongly serpentinized, the thin section of interest still
509 shows relics of primary phases, which enables us to investigate the petrogenesis of this rock. The
510 background rock is a dunite which contains circular to oval clusters of either wehrlitic (only
511 olivine and clinopyroxene) and troctolitic (only olivine and plagioclase) assemblages. It is
512 important to note that these clusters coexist over a cm-scale (Fig. 7d). Considering the
513 interpretation of the phase relations shown in Fig. 9, this special phase situation can be explained
514 by differentiation along path #3 in Fig. 9. This path first crossed the dunitic phase domain
515 (formation of the dunitic matrix) and ended at the point where the saturation curves for
516 plagioclase and clinopyroxene are crossing, where both the troctolitic and the wehrlitic phase
517 assemblage are stable (marked in Fig. 9). At that point very minor changes of bulk composition
518 of water activity could then drag the assemblage into either the wehrlite or troctolite field. If the
519 composition landed exactly on the crossing point the system ends up with a three phase
520 assemblage, which is a bit different from the two distinct lithologies observed in the
521 corresponding sample.

522 Mineral compositions in both the individual clusters and the dunitic matrix in the thin
523 section have been analyzed by electron microprobe. The results are presented in Fig. 7d. Mg#
524 ($\text{MgO}/(\text{MgO}+\text{FeO})$; molar) for olivine in the dunite in the groundmass (83.7), in the wehrlitic
525 domains (83.4), and in the troctolitic domain (83.9) are relatively low, comparable to values from
526 typical Oman gabbros (e.g., MacLeod and Yaouancq, 2000), thus excluding any formation
527 model for wehrlites within this section that involves typical mantle processes. The An content of
528 the plagioclase of the troctolitic domains is very high (89.4 mol%), in agreement with
529 experimental results from hydrous tholeiitic systems. For instance, Feig et al. (2006) recorded a
530 shift in An from nominally dry to water-saturated conditions of > 20 mol% at a given
531 temperature in their experiments. Thus, the very high An content in the troctolitic domains can
532 be used as a strong argument that they formed under high water activities.

533

534 *4.3 The amount of wehrlite and wehrlitic gabbro in OmanDP drill cores*

535 One important question relating to the importance of hydrous magmatic processes at the
536 Oman paleoridge is how common wehrlitic assemblages are within the OmanDP drill cores.
537 Amounts of wehrlite and wehrlitic gabbro (i.e. melagabbro) for the different cores are listed (in
538 % of units) in the proceedings of the OmanDP (Kelemen et al., 2020): CM1: 11.7%, CM2:
539 28.6%, GT1: 3.9%, GT2: 7.9%, GT3: no wehrlites. For CM1 and CM2, the amount of the
540 recorded wehrlite corresponds only to the crustal (gabbroic) part. Thus, the overall amount of
541 wehrlitic rocks within the layered gabbro series is significant, and even in reality higher when the
542 millimeter- to cm-thin wehrlitic layers in layered gabbros series that have been assigned to
543 olivine gabbro units are also considered. From this, it can be concluded that the record of
544 wehrlites all over the drilled transects from the crust/mantle boundary up to the mid-crust where
545 the foliated gabbros become dominant, can be regarded as a clear indication for accretion of the
546 full thickness of the Oman paleocrust under hydrous conditions.

547 Concerning the evolution of wehrlites with crustal height, three observations are
548 significant: (1) The overall amount of wehrlite decreases with crustal height, (2) the thickness of
549 coherent wehrlite layers decreases with crustal height, and (3) wehrlites disappear in the
550 uppermost part of the plutonic crust (in a crustal level between the GT2 and GT3 cores). This can
551 be explained by a decrease in pressure, since the experimentally derived phase relations show a
552 decrease in the stability of the wehrlite assemblage with pressure (Fig. 3d-f). Another possibility
553 could be that compositions develop to more differentiated compositions with crustal height, as
554 shown for gabbros from the EPR (Lissenberg et al., 2013), which also reduces the stability of the
555 wehrlitic phase domain.

556

557 *4.4 Further evidence for wet differentiation during the accretion of the Oman paleoridge:*
558 *elevated An contents in plagioclase*

559 Differentiation paths expressed by An content in plagioclase versus Mg# in clinopyroxenes from
560 gabbros both from the Oman ophiolite and from modern EPR crust are plotted in Fig. 10. In spite
561 of the data's broad scatter, different evolution trends for both areas are visible, as shown in Fig.
562 10. While the EPR sample suites follow straight evolution trends similar to those from other
563 modern mid-oceanic ridges (Coogan, 2014), the trend for the Oman gabbro shows a clear
564 evolution towards enhanced An contents in plagioclase, which can be interpreted as a

565 consequence of higher water activities in the parental melts forming the Oman paleo ridge.
566 However, the Oman trend is significantly different from evolution trends of typical arc gabbros,
567 where the enrichment in An content is much stronger, as shown by the differentiation path for
568 arc gabbros in Fig. 10 (data from Kvassnes et al., 2004). This emphasizes that the magmatic
569 processes which formed the Oman paleo ridge share more similarities with those active at
570 modern fast-spreading mid-ocean ridges like EPR, than with those related to modern arc crust
571 formation.

572 *4.5 Phase diagrams for the AML and application to the gabbros from OmanDP drill core GT3* 573 *penetrating the dike/gabbro transition*

574 The phase diagrams for hydrous MORB systems at 50 MPa allow us to predict
575 crystallization orders for melts freezing in the AML to produce gabbro, i.e., the type of
576 varitextured gabbros (see section 3.3). The phase diagram in 4a is based on pressure dependent
577 experiments in the primitive MORB system performed at fairly oxidizing conditions (varying
578 between QFM~1 at low water activities and QFM+4.2 at water-saturated conditions). A
579 consequence is that this system shows relatively early magnetite saturation, which appears in the
580 diagram of 4a shortly after clinopyroxene, but distinctly before orthopyroxene and amphibole.
581 Since it can be expected that the redox conditions in the real AMLs are lower, the magnetite
582 saturation curve can be significantly lowered or even disappear (Fig. 3a), depending on the
583 prevailing redox conditions and on the composition. On the other hand, when considering more
584 differentiated systems, the magnetite saturation curve will be shifted to higher temperatures, and
585 in that composition, representing a MORB late stage melt, magnetite is even liquidus phase (Fig.
586 3c, 4b), at redox conditions spanning oxygen fugacities from QFM+1 ($a_{\text{H}_2\text{O}} = 1$) to QFM-1
587 ($a_{\text{H}_2\text{O}} < 1$) (Koepke et al., 2018).

588 From the phase diagram for a primitive system at 50 MPa (Fig. 4a) the order of main
589 stage crystallization is olivine – plagioclase – clinopyroxene (ignoring magnetite, see above).
590 The corresponding phase assemblage can be observed in some of the varitextured gabbros of
591 the GT3 cores (e.g., Fig. F27 in the proceedings of GT3 in Kelemen et al., 2020), with olivines
592 being totally serpentinized. It is noteworthy that wehrlitic assemblages have not been observed in
593 the GT3 core, in fully concordance with the corresponding phase diagrams (Fig. 3d-f).
594 Varitextured gabbros without olivine are however much more common, as shown in Fig. 8. The
595 petrographic record shows that plagioclase crystallized before clinopyroxene, followed by the

596 late stage crystallization of interstitial amphibole and Fe-Ti oxide, which does not agree with the
597 phase diagram in 4a, because of the missing olivine. There are at least two possible explanations
598 for this.

599 One explanation is that the system did not crystallize under equilibrium conditions, as
600 was the case for the experiments. Arguments for this are indications for fast crystal growth that
601 can be observed in thin sections (i.e., olivine shows skeletal amoeboid shape; see Fig. F27 in the
602 proceedings of GT3, Kelemen et al., 2020, clinopyroxene shows skeletal structure, and
603 plagioclase forms extreme long crystals often with skeletal morphology). Further arguments for
604 disequilibrium crystallization include reactions observed in thin sections producing amphibole
605 from primary clinopyroxene (see red arrow in Fig. 8), as well as strong plagioclase zoning.

606 Another reason why olivine is only rarely observed in the gabbros from the AML horizon
607 is that the chemistry of the varitextured gabbro shows evolution towards highly differentiated
608 compositions, such that the phase diagram in Fig. 4b for a hydrous late stage MORB system is
609 more relevant than that in Fig. 4a. Here, the crystallization takes place at much lower
610 temperatures, without olivine as liquidus phase. Instead, magnetite is the first phase which
611 crystallizes, which is in agreement with observations of highly differentiated compositions in
612 varitextured gabbros (ferrogabbros; e.g., Müller et al., 2017; MacLeod and Yaouancq, 2000).
613 According to the proceedings for the core GT3 in Kelemen et al. (2020), the varitextured gabbros
614 span a large compositional field, from fairly primitive (bulk Mg# = 75) to highly differentiated
615 ferrogabbros (bulk Mg# ~36). The phase relations observed in the ferrogabbros of the GT3 core
616 fit quite well with the phase diagram in Fig. 4b: the recorded mineral assemblage consists of
617 magnetite, ilmenite, clinopyroxene and plagioclase produced in the main crystallization stage;
618 orthopyroxene is widely absent; up to 2% apatite is present as late stage phase, as well as high
619 amounts of magmatic interstitial hornblende (see proceedings of GT3 in Kelemen et al., 2020).
620

621 *4.6 Implications for the accretion of the lower crust at the Oman paleoridge*

622 The frequency of wehrlitic layers within the deep crust recorded in the OmanDP drill
623 cores prominently reflects the hydrous nature of lower crustal Oman phase-1 magmatism. Here,
624 wehrlites and wehrlitic gabbros document special conditions, where local water activities have
625 been significantly increased, with the consequence that plagioclase crystallization was

626 suppressed. These findings have implications for the mechanism of accretion of the lower crust
627 at the Oman paleoridge.

628 In the gabbro glacier model (see section 1.1) primitive MORB melts are delivered from
629 the mantle to the AML, where differentiation takes place, producing crystals that accumulate in
630 crystal mushes, which fed as crystal-liquid suspension currents the whole lower crust. This
631 model cannot explain wehrlite production within the lower crust according to the model of
632 wehrlite formation established above. Provided a hydrous MORB melt within the axial melt
633 reservoir is water-saturated ($a_{\text{H}_2\text{O}} = 1$), then its maximum water content at a pressure of 50 MPa
634 would be ~ 2.2 wt% (Berndt et al., 2002). When according to the gabbro glacier model crystal-
635 liquid suspension currents starts to move downwards towards higher pressure, the water activity
636 decreases because of the strong dependence of water solubility with depth. At a pressure of 100
637 MPa (the mid-crust) the activity of water in the same melt containing ~ 2.2 wt% water is
638 significantly lower ($a_{\text{H}_2\text{O}} \sim 0.5$). At a pressure of 200 MPa (the lowermost crust), water activity
639 is lowered further ($a_{\text{H}_2\text{O}} \sim 0.3$), which drastically reduces the potential for crystallizing the
640 wehrlite paragenesis (according to Fig. 3 and 9), at a crustal level where the record of wehrlite
641 within the layered gabbro series is greatest. This simple consideration makes it highly unlikely
642 that the gabbro glacier process played a significant role during the accretion of the Oman deep
643 paleocrust.

644 Quite different is the evaluation concerning the other endmember model for fast-spread
645 ocean crust accretion, the sheeted sill model, where the deep crust is formed by in-situ
646 crystallization within relatively small melt sills, injected into the crystal mushes of the lower
647 crust (see section 1.1). When considering that intruding melt volumes have different water
648 contents, wehrlite formation in the deep crust is promoted when the water contents of injected
649 melts are particularly high (Fig. 3 and 9). For most injected melts the water contents were lower,
650 i.e., below the threshold for generating the wehrlite stability, so that "normal" olivine gabbros
651 were produced. Recent results on the isotope geochemistry of sub-nano gram samples from the
652 modern lower oceanic crust revealed that individual melts may have derived from distinct mantle
653 components delivered to the lower crust on a cm scale (Lambart et al., 2019). Hence, it is very
654 probable that individual melt batches also could differ in water contents given the close
655 correlation between water and incompatible trace element contents in MORB-like systems (e.g.,
656 Michael, 1995; Saal et al., 2002).

657 According to the sheeted sill mechanism of Kelemen et al. (1997), residual melts with
658 relatively high water activities (i.e., after precipitating the wehrlitic assemblage) may percolate
659 upwards into the overlying mush stockwork and interact with minerals of olivine gabbro mushes
660 residing there. Since these crystals are then in contact with melts enriched in water, reverse
661 mineral zoning in plagioclase would be expected due to the well-known effect of water activity
662 on plagioclase composition (e.g., Botcharnikow et al., 2018; Feig et al., 2006). Indeed, such a
663 zonation trend in plagioclase towards An-richer rims is common for Oman phase-1 layered
664 gabbros (Browning, 1982; MacLeod and Yaouancq, 2000; Mueller, 2016), supporting this
665 model. It should however be noted that such an inverse zonation of plagioclase is not observed in
666 gabbros recovered from the EPR, which further highlights the hydrous nature of the Oman
667 paleocrust with respect to modern fast-spreading mid-ocean ridges. In principle, a further
668 upward percolation would drive water-rich melts towards water saturation, leading to increasing
669 wehrlite formation with crustal height. However, this is not observed, which we attribute (1) to
670 the mixing of such melts with relatively primitive melts, with lower water contents, and (2) to the
671 lower stability of the wehrlite assemblage with upwards decreasing pressure.

672 In Fig. 11 we present a sketch of our model highlighting the formation of the lower crust
673 in a hydrous MORB system, with focus on wehrlite formation. Central to this is the mode of
674 layer formation in oceanic layered gabbros, which remains poorly understood. The basis for our
675 model is a recent study on layer formation in oceanic gabbros by Mock et al. (2021a), who
676 investigated a two-meter-thick section of a well-known gabbro outcrop in the Wadi Somerah
677 (Sumail massif) that shows decimeter-scale modal layering with olivine abundances gradually
678 decreasing from layer bases to tops, which is the most common type of layering in the Oman
679 lower gabbros. This section was investigated with a high spatial resolution (centimeter-scale) by
680 applying different techniques (EPMA, LA-ICPMS, EBSD, cooling rate speedometry).

681 Overall, Mock et al. (2020a) suggested that layers were deposited by density currents of
682 crystal-laden magma within a melt sill. Crystallization occurred at the cooler margins of the melt
683 reservoirs, before slumping downward to their bases, establishing layering typical for the lower
684 Oman gabbros. The dynamics within such a current might prevent clear trends in grain size and
685 phase density within a layer, as would be expected in an environment of undisturbed crystal
686 settling. Marked changes of the recorded signals, especially in terms of mineral chemistry and
687 microstructures, even within one layer, emphasizes the importance of replenishment during layer
688 formation. Considering this formation model, we assume that replenishments can also include

689 primary melts with elevated water concentrations, which then may increase the water activity of
690 the system, which in turn could result in the formation of pure wehrlite layers. This would be the
691 case if a differentiation path left of arrow #3 shown in Fig 9 jumps to a path right of arrow #3,
692 due to an abrupt increase of water activity in the system. Such processes operating within an
693 individual melt reservoir are shown in Fig. 11b. An overview through crust and uppermost
694 mantle, highlighting the formation of wehrlitic layers in the lower part of the crust is shown in
695 Fig. 11b.

696

697 *4.7 Hydration of the lower crust via deep hydrothermal activity*

698 In the model explained above we assume that the water in Oman parental melts
699 responsible for the formation of coherent wehrlite layers and general enrichment of plagioclase
700 An contents is primary in nature, originating from MORB genesis in an setting of subduction
701 zone initiation transiting between decompression and flux melting of mantle (e.g., Stern, 2004;
702 Agard et al., 2020). However, there are alternative explanations for the involvement of water
703 during the magmatic phase 1 at the Oman paleoridge, which are related to hydrothermal
704 processes operating under very high and even magmatic temperatures. Nicolas et al. (2003)
705 observed a thermally induced microcrack network cutting deep layered gabbros in which very
706 high mineral formation temperatures have been recorded. Isotope investigations on the
707 mineralogical fillings of these cracks revealed seawater-derived hydrothermal fluids (Bosch et
708 al., 2004). Other observations from the lower crust of the Oman ophiolite focus on hydrothermal
709 fault zones, cutting the layered gabbro at several places in the southern massifs of the Oman
710 ophiolite, which have the potential to feed the lower crust with seawater-derived fluids (Coogan
711 et al., 2003; Ziehlman et al., 2018). Results of structural and petrological studies in the Wadi
712 Maharam (Sumail massif) revealed that hydrothermally derived water-rich fluids were
713 introduced via normal faults deep into the lower crust within the magmatic regime, producing
714 hydrous cumulate gabbros with anomalously high An contents in plagioclase (An 90%–95%).
715 Benoit et al. (1999) provided isotopic evidence for the correlation between the high An content
716 of plagioclase and Sr isotopes evidencing the sea-water origin of hydrothermal water-rich fluids
717 involved in the petrogenesis of some depleted gabbroic rocks from dikes in the "Maqsad" mantle
718 diapir (Sumail massif). Moreover, Koepke et al. (2014) showed that gabbros from the Wadi
719 Rajmi in the Northern Oman experienced an invasion of seawater-derived fluids along grain

720 boundaries, which triggered partial melting in these rocks. Finally, Rospabe et al. (2019) present
721 evidence showing that hydrothermal water penetration down to the crust/mantle transition along
722 early faults triggered hydrous rock-forming processes at the base of the crust.

723 All these examples highlight that seawater-derived hydrothermal fluids had the potential
724 to locally penetrate deeply into the plutonic crust during the Oman paleo ridge accretion,
725 catalyzing hydrous magmatism that produced gabbroic rocks anomalous rich in An content of
726 plagioclase. These processes have the potential to remove latent heat of crystallization, which is
727 necessary for enabling in-situ crystallization, following the injection of melt sills into the lower
728 oceanic crust. However, these processes are local phenomena, which cannot account for the
729 widespread enrichment of An content in plagioclases from Oman gabbros (Fig. 10), which is a
730 consequence of elevated primary water contents in the parental melts forming the Oman paleo
731 ridge, due to the tectonic environment of subduction zone initiation.

732 **5 Conclusions**

733 Based on the combined phase relations for hydrous MORB-type systems at shallow pressures
734 and on the petrological record of coherent wehrlites or wehrlitic layers in layered gabbros from
735 phase-1-plutonics recovered by the OmanDP, we draw the following conclusions:

736

- 737 • From the experimentally derived phase relations we conclude that the wehrlitic phase
738 assemblage (olivine coexist with clinopyroxene without plagioclase) is the most significant
739 feature indicative of high prevailing water activities.
- 740 • The phase relations imply that the stability of the wehrlitic assemblage decreases with
741 decreasing pressure (not stable in the upper part of the lower crust) and is depending on the
742 chemical system (only stable in primitive MORB systems).
- 743 • The application of the results of the evaluation of the phase diagrams in hydrous tholeiitic
744 systems at shallow pressures to the natural gabbroic sequences recovered by the OmanDP
745 provide overwhelming evidence that the magmatic accretion of the lower crust of the Oman
746 Ophiolite paleoridge was wet, as consequence of an origin within an environment of
747 subduction zone initiation.
- 748 • While the key petrographic features indicative for the hydrous differentiation at the Oman
749 paleoridge in the lower and mid-crust is the mineral assemblage olivine-clinopyroxene

750 (without plagioclase), it is interstitial amphibole, often in coexistence with Fe-Ti oxides, in
751 the uppermost plutonic crust (dike/gabbro transition).

- 752 • The evaluation of the phase relations in hydrous tholeiitic systems at shallow pressures enable
753 us, to construct phase diagrams for the AML at 50 MPa in a wet system, in order to predict
754 the phase relation in this important melts reservoir.
- 755 • Our results shed light on the detailed mechanism of wehrlite formation within the deep crust
756 as a consequence of the prevailing water activity, highlighting the importance of in-situ
757 crystallization in deep sills during crust accretion.

758
759

760 **Acknowledgement**

761 This work is dedicated to Prof. Adolphe Nicolas, who inspired JK 20 years ago to
762 perform experiments in hydrous systems in order to understand better the magmatic processes at
763 the Oman paleoridge. In the following years, he and Francoise Boudier, introduced JK into the
764 Oman mountains, performing marvelous, unforgettable field campaigns, often together with
765 friends and students from all over the world.

766 Many thanks to the reviewers Georges Ceuleneer and Tomo Morishita, and to the editor
767 Philippe Agard for their comments and suggestions which significantly improved this
768 manuscript.

769 This research used samples and/or data provided by the Oman Drilling Project. The
770 Oman Drilling Project (OmanDP) has been possible through co-mingled funds from the
771 International Continental Scientific Drilling Project (ICDP; Kelemen, Matter, Teagle Lead PIs),
772 the Sloan Foundation – Deep Carbon Observatory (Grant 2014-3-01, Kelemen PI), the National
773 Science Foundation (NSF-EAR-1516300, Kelemen lead PI), NASA – Astrobiology Institute
774 (NNA15BB02A, Templeton PI), the German Research Foundation (DFG: KO 1723/21-1,
775 Koepke PI), the Japanese Society for the Promotion of Science (JSPS no:16H06347,
776 Michibayashi PI; and KAKENHI 16H02742, Takazawa PI), the European Research Council
777 (Adv: no.669972; Jamveit PI), the Swiss National Science Foundation (SNF:20FI21_163073,
778 Früh-Green PI), JAMSTEC, the TAMU-JR Science Operator, and contributions from the
779 Sultanate of Oman Ministry of Regional Municipalities and Water Resources, the Oman Public
780 Authority of Mining, Sultan Qaboos University, CNRS-Univ. Montpellier, Columbia University

781 of New York, and the University of Southampton. This study was funded by DFG projects KO
782 1723/16-1, 21-1, 25-1, and 27-1. DAN acknowledges support from the Natural Environment
783 Research Council (NE/T011106/1).

784

785 **Data Availability**

786 In this paper we compiled the results from four experimental phase equilibria studies, which
787 were all published: Berndt et al. (2005), Feig et al. (2006, 2010) and Koepke et al. (2018). All
788 details to the experiments can be found in these papers. The used rocks are personal samples
789 from J.K. of the drill cores CM1, CM2, GT1, GT2, and GT3 recovered in the frame of the ICDP
790 Oman Drilling Project (OmanDP, <https://www.omandrilling.ac.uk/>). The corresponding cores are
791 stored in the American Museum of Natural History (New York). Samples can be requested from
792 individual researchers via the OmanDP webpage. The core photos are from the supplemental
793 material published on the IODP platform (Kelemen et al., 2020).

794

795 **References**

- 796 Abily, B., Ceuleneer, G., Launeau, P., 2011. Synmagmatic normal faulting in the lower oceanic
797 crust: Evidence from the Oman ophiolite. *Geology* 39, 391-394.
- 798 Agard, P., Prigent, C., Soret, M., Dubacq, B., Guillot, S., Deldicque, D., 2020. Slabitization:
799 Mechanisms controlling subduction development and viscous coupling. *Earth-Science*
800 *Reviews* 208, <https://doi.org/10.1016/j.earscirev.2020.103259>
- 801 Almeev, R., Holtz, F., Koepke, J., Parat, F., Botcharnikov, R., 2007. The effect of H₂O on
802 olivine crystallization in MORB: Experimental calibration at 200 MPa. *American*
803 *Mineralogist* 92, 670-674.
- 804 Anonymous, 1972. Penrose Field Conference: Ophiolites. *Geotimes* 17, 24–25.
- 805 Arai, S., Takemoto, Y., 2007. Mantle wehrlite from Hess Deep as a crystal cumulate from an
806 ultra-depleted primary melt in East Pacific Rise. *Geophysical Research Letters* 34,
807 [doi:10.1029/2006GL029198](https://doi.org/10.1029/2006GL029198).
- 808 Arculus, R.J., Gurnis, M., Ishizuka, O., Reagan, M.K., Pearce, J.A., Sutherland, R., 2019. How
809 to create new subduction zones. A Global Perspective. *Oceanography* 32, 160-174.

- 810 Ariskin, A.A., 1999. Phase equilibria modeling in igneous petrology: use of COMAGMAT
811 model for simulating fractionation of ferro-basaltic magmas and the genesis of high-alumina
812 basalt. *Journal of Volcanology and Geothermal Research* 90, 115-162.
- 813 Beard, A.D., Downes, H., Mason, P.R.D., Vetrin, V.R., 2007. Depletion and enrichment
814 processes in the lithospheric mantle beneath the Kola Peninsula (Russia): Evidence from
815 spinel lherzolite and wehrlite xenoliths. *Lithos* 94, 1-24.
- 816 Benoit, M., Ceuleneer, G., Polve, M., 1999. The remelting of hydrothermally altered peridotite at
817 mid-ocean ridges by intruding mantle diapirs. *Nature* 402, 514-518.
- 818 Berndt, J., Koepke, J., Holtz, F., 2005. An experimental investigation of the influence of water
819 and oxygen fugacity on differentiation of MORB at 200 MPa. *Journal of Petrology* 46, 135-
820 167.
- 821 Berndt, J., Liebske, C., Holtz, F., Freise, M., Nowak, M., Ziegenbein, D., Hurkuck, D., Koepke,
822 J., 2002. A combined rapid-quench and H₂-membrane setup for internally heated pressure
823 vessels: Description and application for water solubility in basaltic melts. *American*
824 *Mineralogist* 87, 1717-1726.
- 825 Bézoz, A., Humler, E., 2005. The Fe³⁺/ΣFe ratios of MORB glasses and their implications for
826 mantle melting. *Geochimica et Cosmochimica Acta* 69, 711-725.
- 827 Bosch, D., Jamais, M., Boudier, F., Nicolas, A., Dautria, J-M., Agrinier, P., 2004. Deep and
828 high-temperature hydrothermal circulation in the Oman ophiolite - Petrological and isotopic
829 evidence. *Journal of Petrology* 45, 1181-1200.
- 830 Botcharnikov, R.E., Almeev, R., Koepke, J., Holtz, F., 2008. Phase relations and liquid lines of
831 descent in hydrous ferrobalt - Implications for the Skaergaard Intrusion and Columbia
832 River Flood Basalts. *Journal of Petrology* 49, 1687-1727.
- 833 Botcharnikov, R.E., Koepke, J., Holtz, F., McCammon, C., Wilke, M., 2005. The effect of water
834 activity on the oxidation and structural state of Fe in a ferro-basaltic melt. *Geochimica et*
835 *Cosmochimica Acta* 69, 5071-5085.
- 836 Browning, P., 1982. The petrology, geochemistry, and the structure of the plutonic rocks of the
837 Oman ophiolite. Open University, p. 404.
- 838 Canales, J.P., Detrick, R.S., Toomey, D.R., Wilcock, W.S.D., 2003. Segment-scale variations in
839 the crustal structure of 150-300 kyr old fast spreading oceanic crust (East Pacific Rise, 8
840 degrees 15 ' N-10 degrees 5 ' N) from wide-angle seismic refraction profiles. *Geophys. J. Int.*
841 152, 766-794.

- 842 Canales, J.P., Nedimovic, M.R., Kent, G.M., Carbotte, S.M., Detrick, R.S., 2009. Seismic
843 reflection images of a near-axis melt sill within the lower crust at the Juan de Fuca ridge.
844 *Nature* 460, 89-U100.
- 845 Carbotte, S. M., Marjanović, M., Arnulf, A. F., Nedimović, M. R., Canales, J. P., Arnoux, G. M.,
846 2021. Stacked Magma Lenses Beneath Mid-Ocean Ridges: Insights From New Seismic
847 Observations and Synthesis With Prior Geophysical and Geologic Findings. *Journal of*
848 *Geophysical Research: Solid Earth* 126, e2020JB021434.
- 849 Constantin, M., Hékinian, R., Bideau, D., Hébert, R. j. (1996). Construction of the oceanic
850 lithosphere by magmatic intrusions: Petrological evidence from plutonic rocks formed along
851 the fast-spreading East Pacific Rise. *Geology* 24, 731-734.
- 852 Coogan, L. A., Howard, K. A., Gillis, K. M., Bickle, M. J., Chapman, H., Boyce, A. J., . . .
853 Wilson, R. N., 2006. Chemical and thermal constraints on focussed fluid flow in the lower
854 oceanic crust. *American Journal of Science* 306, 389-427, doi:10.2475/06.2006.01
- 855 Coogan, L.A., 2014. The lower oceanic crust; 2nd Edition, in: Turekian, K., Holland, H.D.
856 (Eds.), *Treatise on Geochemistry*. Elsevier, Amsterdam, pp. 497-541.
- 857 Cottrell, E., Birner, S., Brounce, M., Davis, F.A., Waters, L.E., Kelley, K.A., 2021 in press.
858 Oxygen Fugacity Across Tectonic Settings. AGU Geophysical Monograph, in: Neuville,
859 D.R., Moretti, R. (Eds.), *Redox variables and mechanisms in magmatism and volcanism*.
860 Wiley, p. DOI: 10.1002/essoar.10502445.10502441.
- 861 Cowan, R.J., Searle, M.P., Waters, D.J., 2014. Structure of the metamorphic sole to the Oman
862 Ophiolite, Sumeini Window and Wadi Tayyin: implications for ophiolite obduction
863 processes, in: Rollinson, H.R., Searle, M.P., Abbasi, I.A., Al-Lazki, A., Al-Kindi, M.H.
864 (Eds.), *Tectonic Evolution of the Oman Mountains*. Geological Society of London, Special
865 Publication, Vol. 392, London, pp. 155-175, doi: 110.1144/SP1392.1148.
- 866 Crawford, A.J., Falloon, T.J., Eggins, S., 1987. The origin of island-arc High-Alumina basalts.
867 *Contributions to Mineralogy and Petrology* 97, 417-430.
- 868 Danyushevsky, L.V., 2001. The effect of small amounts of H₂O crystallisation of mid-ocean
869 ridge and backarc basin magmas. *Journal of Volcanology and Geothermal Research* 110,
870 265-280.
- 871 de Graaff, S.J., Goodenough, K.M., Klaver, M., Lissenberg, C.J., Jansen, M.N., Millar, I.,
872 Davies, G.R., 2019. Evidence for a Moist to Wet Source Transition Throughout the Oman-

- 873 UAE Ophiolite, and Implications for the Geodynamic History. *Geochemistry Geophysics*
874 *Geosystems* 20, 651-672.
- 875 Dick, H. J. B., Natland, J. H. (1996). Late-stage melt evolution and transport in the shallow
876 mantle beneath the East Pacific Rise. *Proc. ODP, Sci. Results* 147, 103 -134.
- 877 Elthon, D., 1991. Experimental phase petrology of mid-ocean ridge basalts, in: Floyd, P.A. (Ed.),
878 *Oceanic basalts*. Blackie, New York, pp. 94-115.
- 879 Ernst, W.G., Liu, J., 1998. Experimental phase-equilibrium study of Al- and Ti-contents of calcic
880 amphibole in MORB - a semiquantitative thermobarometer. *American Mineralogist* 83, 952-
881 969.
- 882 Feig, S., Koepke, J., Snow, J., 2006. Effect of water on tholeiitic basalt phase equilibria: An
883 experimental study under oxidizing conditions. *Contributions to Mineralogy and Petrology*
884 152, 611-638.
- 885 Feig, S., Koepke, J., Snow, J.E., 2010. Effect of oxygen fugacity and water on phase equilibria of
886 a hydrous tholeiitic basalt. *Contributions to Mineralogy and Petrology* 159, doi:
887 10.1007/s00410-00010-00493-00413.
- 888 Gaetani, G.A., Grove, T.L., Bryan, W.B., 1993. The influence of water on the petrogenesis of
889 subduction-related igneous rocks. *Nature* 365, 332-334.
- 890 Ghiorso, M.S., Sack, R.O., 1995. Chemical mass transfer in magmatic processes. IV. A revised
891 and internally consistent thermodynamic model for the interpolation and extrapolation of
892 liquid-solid equilibria in magmatic systems at elevated temperatures and pressures.
893 *Contributions to Mineralogy and Petrology* 84, 107-145.
- 894 Gillis, K.M., Snow, J.E., Klaus, A., and the Expedition 345 Scientists, 2014. Expedition 345.
895 *Proceedings of the Integrated Ocean Drilling Program* 345.
- 896 Godard, M., Dautria, J.-M., Perrin, M., 2003. Geochemical variability of the Oman ophiolite
897 lavas: Relationship with spatial distribution and paleomagnetic directions. *Geochemistry*
898 *Geophysics Geosystems* 4, 2002GC000452.
- 899 Grove, T. L., Kinzler, R. J., Bryan, W. B., 1992. Fractionation of Midoceanic Ridge Basalt
900 (MORB). in Morgan, J. P., Blackman, D. K., Sinton, J. M. (eds.): *Mantle Flow and Melt*
901 *Generation at Mid-Ocean Ridges*, *Geophysical Monograph Series* 71, 281-310.
- 902 Guilmette, C., Smit, M.A., van Hinsbergen, D.J.J., Gurer, D., Corfu, F., Charette, B., Maffione,
903 M., Rabeau, O., Savard, D., 2018. Forced subduction initiation recorded in the sole and crust
904 of the Semail Ophiolite of Oman. *Nature Geoscience* 11, 688-+.

- 905 Henstock, T.J., Woods, A.W., White, R.S., 1993. The accretion of oceanic-crust by episodic sill
906 Intrusion. *Journal of Geophysical Research-Solid Earth* 98, 4143-4161.
- 907 Holness, M.B., 2014. The effect of crystallization time on plagioclase grain shape in dolerites.
908 *Contributions to Mineralogy and Petrology* 168.
- 909 Kelemen, P.B., Koga, K., Shimizu, N., 1997. Geochemistry of gabbro sills in the crust-mantle
910 transition zone of the Oman ophiolite: Implications for the origin of the oceanic lower crust.
911 *Earth and Planetary Science Letters* 146, 475-488.
- 912 Kelemen, P.B., Matter, J.M., Teagle, D.A.H., Coggon, J.A., and the Oman Drilling Project
913 Science Team, 2020. Proceedings of the Oman Drilling Project: College Station, TX
914 (International Ocean Discovery Program), <https://doi.org/10.14379/OmanDP.proc.12020>.
- 915 Koepke, J., Botcharnikov, R., Natland, J.H., 2018. Crystallization of late-stage MORB under
916 varying water activities and redox conditions: Implications for the formation of highly
917 evolved lavas and oxide gabbro in the ocean crust. *Lithos*
918 <https://doi.org/10.1016/j.lithos.2018.10.001>.
- 919 Koepke, J., France, L., Müller, T., Faure, F., Goetze, N., Dziony, W., Ildefonse, B., 2011.
920 Gabbros from IODP Site 1256 (Equatorial Pacific): Insight into axial magma chamber
921 processes at fast-spreading ocean ridges *Geochemistry Geophysics Geosystems* 12,
922 doi:10.1029/2011GC003655.
- 923 Koepke, J., Berndt, J., Horn, I., Fahle, J., Wolff, P.E., 2014. Partial melting of oceanic gabbro
924 triggered by propagating water-rich fluids: a prime example from the Oman ophiolite. In:
925 H.R. Rollinson, M.P. Searle, I.A. Abbasi, A. Al-Lazki and M.H. Al-Kindi (Editors),
926 *Tectonic Evolution of the Oman Mountains*. Geological Society of London, Special
927 Publication 392, London, 187-204.
- 928 Koepke, J., Schoenborn, S., Oelze, M., Wittmann, H., Feig, S., Hellebrand, E., Boudier, F.,
929 Schoenberg, R., 2009. Petrogenesis of crustal wehrlites in the Oman ophiolite: Experiments
930 and natural rocks. *Geochemistry Geophysics Geosystems* 10, doi:10.1029/2009GC002488.
- 931 Koepke, J., Zhang, C., 2021. Axial melt lens dynamics at fast-spreading mid-ocean ridges, in:
932 Vetere, F. (Ed.), *Dynamic Magma Evolution*. AGU Geophysical Monograph, Vol. 254.
933 Wiley, pp. ISBN: 978-971-119-52113-52116.
- 934 Koga, K.T., Kelemen, P.B., Shimizu, N., 2001. Petrogenesis of the crust-mantle transition zone
935 and the origin of lower crustal wehrlite in the Oman ophiolite. *Geochemistry Geophysics*
936 *Geosystems* 2, 2000GC000132.

- 937 Kuno, H., 1960. High-alumina Basalt. *Journal of Petrology* 1, 121–145,
938 <https://doi.org/10.1093/petrology/1.2.121>.
- 939 Kvassnes, A. J. S., Strand, A. H., Moen-Eikeland, H., Pedersen, R. (2004). The Lyngen Gabbro:
940 The lower crust of an Ordovician Incipient Arc. *Contributions to Mineralogy and Petrology*
941 148, 358-379.
- 942 Lambart, S., Koornneef, J.M., Millet, M.-A., Davies, G.R., Cook, M., Lissenberg, C.J., 2019.
943 Highly heterogeneous depleted mantle recorded in the lower oceanic crust. *Nature*
944 *Geoscience* 12, 482-+.
- 945 le Roux, P.J., Shirey, S.B., Hauri, E.H., Perfit, M.R., Bender, J.F., 2006. The effects of variable
946 sources, processes and contaminants on the composition of northern EPR MORB (8-10
947 degrees N and 12-14 degrees N): Evidence from volatiles (H₂O, CO₂, S) and halogens (F,
948 Cl). *Earth and Planetary Science Letters* 251, 209-231.
- 949 Lippard, S.J., Shelton, A.W., Gass, I.G., 1986. *The ophiolite of Northern Oman*. Blackwell
950 Scientific Publ., Oxford.
- 951 Lissenberg, C. J., MacLeod, C. J., Howard, K. A., Godard, M. (2013). Pervasive reactive melt
952 migration through fast-spreading lower oceanic crust (Hess Deep, equatorial Pacific Ocean).
953 *Earth and Planetary Science Letters* 361, 436-447. doi:10.1016/j.epsl.2012.11.012
- 954 MacLennan, J., 2008. Concurrent Mixing and Cooling of Melts under Iceland. *Journal of*
955 *Petrology* 49, 1931-1953.
- 956 MacLeod, C.J., Lissenberg, C.J., Bibby, L.E., 2013. "Moist MORB" axial magmatism in the
957 Oman ophiolite: The evidence against a mid-ocean ridge origin. *Geology* 41, 459-462.
- 958 MacLeod, C.J., Yaouancq, G., 2000. A fossil melt lens in the Oman ophiolite: Implications for
959 magma chamber processes at fast spreading ridges. *Earth and Planetary Sciences Letters*
960 176, 357-373.
- 961 Michael, P.J., 1995. Evidence from trace elements and H₂O for regionally distinctive sources of
962 depleted MORB: Implications for evolution of the depleted mantle. *Earth and Planetary*
963 *Science Letters*, 131, 301–320; doi:10.1180/minmag.1994.58A.2.52.
- 964 Miller, D. J., Iturrino, G. J., Christensen, N. I. (1996). Geochemical and petrological constraints
965 on velocity behavior of lower crustal and upper mantle rocks from the fast-spreading ridge at
966 Hess Deep. *Proc. ODP, Sci. Results* 147, 477-490.

- 967 Mock, D., Neave, D.A., Muller, S., Garbe-Schonberg, D., Namur, O., Ildefonse, B. and Koepke,
968 J., 2021a. Formation of Igneous Layering in the Lower Oceanic Crust From the Samail
969 Ophiolite, Sultanate of Oman. *J. Geophys. Res.-Solid Earth*, 126(1): 29.
- 970 Mock, D., Ildefonse, B., Muller, T., Koepke, J., 2021b. A Reference Section Through Fast-
971 Spread Lower Oceanic Crust, Wadi Gideah, Samail Ophiolite (Sultanate of Oman): Insights
972 From Crystallographic Preferred Orientations. *J. Geophys. Res.-Solid Earth* 126(6): 27.
- 973 Müller, T., 2016. A petrological and geochemical cross section of lower crust at the Wadi
974 Gideah (Samail ophiolite): Implications for the crustal accretion at fast-spreading mid-ocean
975 ridges. University of Hannover, p. 199.
- 976 Müller, T., Koepke, J., Garbe-Schonberg, C.D., Dietrich, M., Bauer, U., Wolff, P.B., 2017.
977 Anatomy of a frozen axial melt lens from a fast-spreading paleo-ridge (Wadi Gideah, Oman
978 ophiolite). *Lithos* 272, 31-45.
- 979 Natland, J. H., Dick, H. J. B. (1996). Melt migration through high-level gabbroic cumulates of
980 the East Pacific Rise at Hess Deep: the origin of magma lenses and the deep crustal structure
981 of fast-spreading ridges. *Proc. ODP, Sci. Results* 147, 21-58.
- 982 Neave, D.A., Namur, O., Shorttle, O., Holtz, F., 2019. Magmatic evolution biases basaltic
983 records of mantle chemistry towards melts from recycled sources. *Earth and Planetary
984 Science Letters* 520, 199-211.
- 985 Nicolas, A., Boudier, F., 2000. Large mantle upwellings and related variations in crustal
986 thickness in the Oman ophiolite. *Geological Society of America Special Paper* 349, 67–73.
- 987 Nicolas, A., Boudier, F., Ildefonse, B., Ball, E., 2000. Accretion of Oman and United Arab
988 Emirates ophiolite - Discussion of a new structural map. *Marine Geophysical Researches* 21,
989 147-179.
- 990 Nicolas, A., Mainprice, D., Boudier, F., 2003. High temperature seawater circulation throughout
991 crust of oceanic ridges. A model derived from the Oman ophiolite. *Journal of Geophysical
992 Research* 108, No. B8.
- 993 O'Neill, H.S.C., Berry, A.J., and Mallmann, G., 2018. The oxidation state of iron in Mid-Ocean
994 Ridge Basaltic (MORB) glasses: Implications for their petrogenesis and oxygen fugacities.
995 *Earth and Planetary Science Letters*, 504, 152–162, doi:10.1016/j.epsl.2018.10.002.
- 996 Pallister, J. S., Hopson, C. A. (1981). Samail Ophiolite plutonic suite: Field relations, phase
997 variation, cryptic variation and layering, and a model of a spreading ridge magma chamber.

- 998 Journal of Geophysical Research: Solid Earth 86(B4), 2593-2644.
999 doi:10.1029/JB086iB04p02593
- 1000 Parkinson, I.J., Arculus, R.J., Eggins, S.M., 2003. Peridotite xenoliths from Grenada, Lesser
1001 Antilles Island Arc. *Contributions to Mineralogy and Petrology* 146, 241-262.
- 1002 Perk, N. W., Coogan, L. A., Karson, J. A., Klein, E. M., Hanna, H. D. (2007). Petrology and
1003 geochemistry of primitive lower oceanic crust from Pito Deep: implications for the accretion
1004 of the lower crust at the Southern East Pacific Rise. *Contributions to Mineralogy and
1005 Petrology* 154, 575-590. doi:10.1007/s00410-007-0210-z
- 1006 Peslier, A.H., Francis, D., Ludden, J., 2002. The lithospheric mantle beneath continental
1007 margins: Melting and melt-rock reaction in Canadian Cordillera xenoliths. *Journal of
1008 Petrology* 43, 2013-2047.
- 1009 Python, M., Ceuleneer, G., Arai, S. 2008. Chromian spinels in mafic–ultramafic mantle dykes:
1010 Evidence for a two-stage melt production during the evolution of the Oman ophiolite. *Lithos*
1011 106, 137–154.
- 1012 Rospabe, M., Benoit, M., Ceuleneer, G., Kaczmarek, M.A., Hodel, F., 2019. Melt hybridization
1013 and metasomatism triggered by syn-magmatic faults within the Oman ophiolite: A clue to
1014 understand the genesis of the dunitic mantle-crust transition zone. *Earth Planet. Sci. Lett.*
1015 516, 108-121.
- 1016 Rioux, M., Bowring, S., Kelemen, P., Gordon, S., Dudas, F., Miller, R., 2012. Rapid crustal
1017 accretion and magma assimilation in the Oman-UAE ophiolite: High precision U-Pb zircon
1018 geochronology of the gabbroic crust. *Journal of Geophysical Research-Solid Earth* 117.
- 1019 Rioux, M., Bowring, S., Kelemen, P., Gordon, S., Miller, R., Dudas, F., 2013. Tectonic
1020 development of the Samail ophiolite: High-precision U-Pb zircon geochronology and Sm-Nd
1021 isotopic constraints on crustal growth and emplacement. *Journal of Geophysical Research-
1022 Solid Earth* 118, 2085-2101.
- 1023 Saal, A.E., Hauri, E.H., Langmuir, C.H., Perfit, M.R., 2002. Vapour undersaturation in primitive
1024 mid-ocean-ridge basalt and the volatile content of Earth's upper mantle. *Nature* 419, 451-
1025 455.
- 1026 Saper, L., Liang, Y., 2014. Formation of plagioclase-bearing peridotite and plagioclase-bearing
1027 wehrlite and gabbro suite through reactive crystallization: an experimental study.
1028 *Contributions to Mineralogy and Petrology* 167, doi:10.1007/s00410-014-0985-7

- 1029 Shaw, C.S.J., Eyzaguirre, J., Fryer, B., Gagnon, J., 2005. Regional variations in the mineralogy
1030 of metasomatic assemblages in mantle xenoliths from the West Eifel Volcanic Field,
1031 Germany. *Journal of Petrology* 46, 945-972.
- 1032 Sisson, T.W., Grove, T.L., 1993. Experimental investigations of the role of H₂O in calc-alkaline
1033 differentiation and subduction zone magmatism. *Contributions to Mineralogy and Petrology*
1034 113, 143-166.
- 1035 Stern, R.J., 2004. Subduction initiation: spontaneous and induced. *Earth and Planetary Science*
1036 *Letters* 226, 275-292.
- 1037 Tormey, D.R., Grove, T.L., Bryan, W.B., 1987. Experimental petrology of normal MORB near
1038 the Kane Fracture Zone: 22°-25° N, Mid-Atlantic Ridge. *Contributions to Mineralogy and*
1039 *Petrology* 96, 121-139.
- 1040 VanTongeren, J. A. (2021). The composition of the lower oceanic crust in the Wadi Khafifah
1041 section of the southern Samail (Oman) ophiolite. Retrieved from:
1042 <https://doi.org/10.5061/dryad.c59zw3r6v>.
- 1043 Vera, E.E., Mutter, J.C., Buhl, P., Orcutt, J.A., Harding, A.J., Kappus, M.E., Detrick, R.S.,
1044 Brocher, T.M., 1990. The structure of 0-my to 0.2-my old oceanic crust at 9° N on the East
1045 Pacific Rise from expanded spread profiles. *Journal of Geophysical Research-Solid Earth*
1046 *and Planets* 95, 15529-15556.
- 1047 Wanless, V.D., Shaw, A.M., 2012. Lower crustal crystallization and melt evolution at mid-ocean
1048 ridges. *Nature Geoscience* 5(9), 651-655.
- 1049 Zihlmann, B., Müller, S., Coggon, R. M., Koepke, J., Garbe-Schönberg, D., & Teagle, D. A. H.,
1050 2018. Hydrothermal fault zones in the lower oceanic crust: An example from Wadi Gideah,
1051 Samail ophiolite, Oman. *Lithos* 323, 103-124. doi:10.1016/j.lithos.2018.09.008
- 1052 Zhang, H.L., Cottrell, E., Solheid, P.A., Kelley, K.A., and Hirschmann, M.M., 2018.
1053 Determination of Fe³⁺/ΣFe of XANES basaltic glass standards by Mössbauer spectroscopy
1054 and its application to the oxidation state of iron in MORB. *Chemical Geology*. 479, 166–
1055 175, doi:10.1016/j.chemgeo.2018.01.006.

1056

1057 **Figures captions**

1058 **Fig. 1.** Schematic section through the Oman ophiolite showing the products of phase-1
1059 magmatism (left) and phase-2 magmatism, the late-stage intrusives (right). "Melt lens" stands for

1060 frozen AML lithologies which are mostly represented by isotropic gabbros (varitextured). "Moho
1061 TZ" stands for Moho Transition Zone.

1062
1063 **Fig. 2.** Images from outcrops in the Oman Ophiolite related to the magmatic phase 1 (a – d) and
1064 phase 2 (e – h) during ocean crust accretion. (a) Layered gabbro in the Wadi Haylayn. (b)
1065 Isotropic gabbro with cm-long hornblende needles in the Wadi Haymilyah. (c) Sheeted dikes in
1066 the Wadi Scheik. (d) Pillow basalts in the Wadi Jizzi. (e) Black wehrlites crosscutting layered
1067 gabbros in the Wadi Haylan. (f) Gabbronorite (left) crosscutting layered gabbro with steep
1068 layering (right) in the Wadi Haymilyah. (g) Large plagiogranite intrusion within upper gabbros
1069 near the Somerah oasis. (h) V2 lava flow showing columnar jointing with clinopyroxene-phyric
1070 basalts in the Wadi Jizzi.

1071
1072 **Fig. 3.** Phase diagrams for different hydrous MORB-type systems performed at shallow
1073 pressures addressing the phase relations in axial magma chambers from the Oman paleoridge and
1074 from other spreading centers in a similar geotectonic setting in an environment of subduction
1075 zone initiation. (a) to (c): results of experiments in different MORB-type systems performed at
1076 200 MPa. (a) Primitive natural MORB from Feig et al. (2010). (b) Model MORB from Berndt et
1077 al. (2005). (c) MORB late stage system (Fe-Ti basalt) from Koepke et al. (2018). (b) and (c) are
1078 redrawn with water content in the melt on the x-axis. (d) to (f): Primitive natural MORB from
1079 Feig et al. (2006) performed at different pressures (100, 200, 500 MPa). Due to the fH_2 buffering
1080 of the experiments in the used experimental equipment (IHPV), fO_2 varies in the experiments,
1081 depending on the prevailing water activity in the individual runs. This is demonstrated in the
1082 experiments shown in (d) to (f), by the dotted vertical lines, where fO_2 varies between QFM+1
1083 for the more dry, and QFM+4.2 for the runs at water saturation. A similar range is given for the
1084 diagrams (a) to (c), which are performed under more reducing conditions (maximum fO_2 of
1085 QFM+2). The phase saturation curves correspond to the appearance (+) and disappearance (-,
1086 dotted) of phases in the corresponding experiments. Abbreviations: Ol - olivine, Cr-sp -
1087 chromium-rich spinel, Cpx - clinopyroxene, Opx - orthopyroxene, Plag - plagioclase, Mag -
1088 magnetite, Amph - amphibole, Ap - apatite, Ilm -ilmenite. The yellow field marks the stability of
1089 the wehrlite assemblage (olivine coexist with clinopyroxene without plagioclase). For details see
1090 text.

1091

1092 **Fig. 4.** Phase diagrams for hydrous MORB-type systems in the axial melt lens of fast-spreading
1093 mid-ocean ridges (50 MPa). Two chemical systems are shown: (a) Primitive natural MORB from
1094 Feig et al. (2006) corresponding to an early stage of differentiation; (b) MORB late stage system
1095 from Koepke et al. (2018) corresponding to a highly evolved MORB system (Fe-Ti basalt). For
1096 explanation of the curves and for abbreviations see Fig. 3. The dashed lines with arrows
1097 correspond to typical differentiation paths. For details see text.

1098

1099 **Fig. 5.** Images from cores drilled within the ICDP OmanDP program showing wehrlite layers
1100 within series of layered gabbroic host rocks. The drill cores are from transects through the
1101 crust/mantle boundary (CM1, a, b), through the layered gabbros (GT1, c), and through the
1102 transition between layered and foliated gabbro (GT2, d). Olivine is in all sections strongly
1103 serpentinized leading to blackish colors. (a) Layered series with alternating layers of olivine
1104 gabbro and wehrlite. (b) Boundary between wehrlite (top) and olivine gabbro (bottom). Note that
1105 the clinopyroxenes in the wehrlite show poikilitic structures, with small olivine chadacrysts.
1106 From such a lithology is thin section image shown in Fig. 6 a. (c) Coarser grained coherent
1107 wehrlite layers within finer grained olivine gabbro showing serpentinite veins parallel to the
1108 direction of layering. (d) Boundary between wehrlitic gabbro (top) and olivine-bearing gabbro
1109 (bottom), with smooth, sutured contact. The scale can be derived from the sample name
1110 presented below the images, where the last numbers indicate the length of the shown section in
1111 cm (code for sample name: Hole#_core#_section#, cm top – cm bottom). The core fotos are from
1112 the supplemental material published on the IODP platform (Kelemen et al., 2020).

1113

1114 **Fig. 6.** Microphotographs from thin section showing wehrlites in the cores recovered in the
1115 frame of the ICDP OmanDP program, from the crust mantle boundary (cores CM1 and CM2),
1116 the deep crust (GT1, representing layered gabbros), and the mid crust (GT2, representing the
1117 transition between layered and foliated gabbros). (a) Wehrlite of drill core CM1 consisting of
1118 exclusively olivine and clinopyroxene. Note the poikilitic structure of the clinopyroxenes,
1119 bearing chadacrysts of small olivines (mostly serpentinized); the interstitial areas with whitish
1120 color correspond to serpentinite. Sample CM1_58_4, 47-51 cm. (b) Massive layered wehrlites of
1121 drill core CM2 with coherent wehrlite layers. The sample is moderately altered. Sample
1122 CM2_104_3, 0-2 cm. (c) Coherent wehrlite layer in layered gabbros of the drill core GT1. This
1123 rock consists of prismatic olivine and clinopyroxene with a few percent of interstitial plagioclase

1124 in the mode, implying a crystallization order of co-crystallization of olivine and clinopyroxene
1125 and late crystallization of plagioclase. Sample GT1_38_4, 36-40 cm. (d) Coherent layers of
1126 wehrlite (upper part) and olivine-bearing gabbro (lower part) in layered gabbros of drill core
1127 GT2, which penetrated the transition between layered and foliated gabbro in the mid-crust. The
1128 wehrlite consists of clinopyroxene and olivine, which is totally altered to iddingsite. A late
1129 serpentinite vein crosscuts both lithologies. Abbreviations: ol - olivine, cpx - clinopyroxene, plag
1130 - plagioclase. Sample GT2_81_4, 38-43 cm.

1131
1132 **Fig. 7.** Images from a section of the OmanDP drill core CM1 (transect through the crust/mantle
1133 boundary) and related microphotographs. (a) Section CM1_18_2, 6-26 cm showing the evolution
1134 from olivine gabbro to a dunitic zone with co-existing circular to oval clusters of wehrlitic and
1135 troctolitic assemblages highlighted in the microphotographs in (b) to (d). (b, c) microphotographs
1136 from clusters with troctolitic (b) and wehrlitic (c) parageneses shown in (d). (d) Thin section foto
1137 from the dunitic zone with troctolitic and wehrlitic clusters shown in (a). Averages of mineral
1138 compositions for individual clusters and for the dunitic matrix are shown (Mg# for olivine, ol,
1139 and clinopyroxene, cpx; An content for plagioclase, pl). Note the extremely high An content of
1140 89.4 mol% which is typical for hydrous systems. The thin section is from a deeper area
1141 (CM1_18_2, 62-67 cm) not shown in (a). The core foto in (a) and the whole thins section foto in
1142 (d) are modified images from the supplemental material published on the IODP platform
1143 (Kelemen et al., 2020).

1144
1145 **Fig. 8.** Microphotograph of a varitextured gabbro from Oman DP drill core GT3 (transect
1146 through dike-gabbro transition); parallel (a) and crossed (b) polarizers. Shown is an example of a
1147 domain with granular texture with late magmatic brown poikilitic amphibole enclosing small
1148 plagioclase crystals. The brown amphibole is of magnesiohastingsitic composition, which is in
1149 the outer parts hydrothermally altered to green hornblende and actinolite. As formation
1150 temperature, 970 °C has been estimated with the Ti-in-amphibole geothermometer of Ernst and
1151 Liu (1998). The red arrow points to a relic of clinopyroxene within the amphibole. Abbreviations
1152 like in Fig. 6 plus am – amphibole. Sample GT3_130-2,12-18 cm.

1153
1154 **Fig. 9.** Detail of the phase diagram shown in Fig. 3 e, for a hydrous primitive natural MORB
1155 system based on crystallization experiments performed by Feig et al. (2006) at 200 MPa with

1156 focus on the main stage crystallization, ignoring the saturation curves of spinel, orthopyroxene,
1157 amphibole, and magnetite. The included lithologies correspond to potential cumulate rocks
1158 which could be formed by phase accumulation according to the stability fields of the phases.
1159 Possible differentiation paths are included: Paths #1 for "dry" parental melts; path #2 for a
1160 condition with a high water concentration, enabling a high water activity; path #3 touches both
1161 the troctolite and the wehrlite field, and explains the phase situation shown in Fig. 7 (both
1162 wehrlitic and troctolitic domains are stable). For details see text.

1163
1164 **Fig. 10.** Chemical mineral evolution expressed by An content in plagioclase versus Mg# in
1165 clinopyroxenes for gabbros from the Oman ophiolite and from EPR crust. The data for Oman are
1166 from Müller (2016, Wadi Gideah), VanTongeren (2021, Wadi Kafifah), Browning (1982, Wadi
1167 Abyad), and Pallister and Hopson (1981, Ibra area). The data for Hess Deep are from Dick and
1168 Natland (1996), Miller et al. (1996), Natland and Dick (1996), and Lissenberg et al. (2013); those
1169 from Pito Deep are from Perk et al. (2007), and Constantin et al. (1996). Data from IODP Hole
1170 1256D are from Koepke et al. (2011). Included are also evolution paths for gabbros from Oman
1171 and EPR, as well as for typical arc gabbros which is based on data presented in Kvassnes et al.
1172 (2004). For details see text.

1173
1174 **Fig. 11.** Sketch of our model highlighting the magmatic formation of the lower crust at the Oman
1175 paleo ridge in a hydrous MORB system, with focus on wehrlite formation. (a) Overview through
1176 the plutonic crust and uppermost mantle, highlighting the formation of wehrlitic layers in the
1177 lower two third of the crust, which are formed by injected melt sills after the model of Kelemen
1178 et al. (1997). In this model, differentiated melt within an individual sill is pressed out due to
1179 compaction and moves upward, resulting in an upward differentiation trend for the lower crust.
1180 Due to the dependence on pressure and composition, the wehrlite formation is strongest at the
1181 base of the crust fading out upward. Deep gabbro sills injected into the mantle are also included,
1182 which may contain layers of wehrlite (Koga et al, 2001). The upper third of the plutonic crust
1183 follows a different mode of emplacement by crystal mush suspensions originating from the axial
1184 melt lens, according to recent results of Mock et al. (2021b), which are based on microstructural
1185 data obtained from rock samples of a profile through the whole lower crust in the Wadi Gideah
1186 (Wadi Tayin massif, Oman ophiolite). The AML is fed with primitive melt delivered from the
1187 upper mantle by a central melt channel. From here, the upper third of the crust is accreted by

1188 downward crystal mush flows (white dashed arrows). According to Mock et al. (2021b) the
1189 lower gabbros consists of layered gabbros and a the lower part of the foliated gabbros, and the
1190 upper gabbros of the upper part of the foliated gabbros and varitextured gabbros. The arrows left
1191 show the lithostatic pressure and the pressure dependent water solubility according to Berndt et
1192 al. (2002). Size of the sills is out of scale; km b.s.: km below seafloor. (b) Detail of the
1193 mechanism of the formation of coherent wehrlite layers within one melt sill, based on the model
1194 for layer formation within deep oceanic gabbros of Mock et al. (2020a), suggesting that
1195 individual layers are deposited by density currents of crystal-laden magma within a melt sill.
1196 Crystallization occurred at the cooler margins of the melt reservoirs, before slumping downward
1197 to their bases, establishing the layering typical for deep gabbros accreted at fast-spreading ridge
1198 systems. At the initial time $t = 0$, a layer of olivine gabbro is produced by crystallization of
1199 hydrous parental MORB left of path #3 in Fig. 9. At $t = 1$, through replenishment, a MORB melt
1200 significantly enriched in water enters the system, which then increases the water activity of the
1201 system, which in turn result in the formation of pure wehrlite layers according to a differentiation
1202 path right of path #3 in Fig. 9. At $t = 2$, a further replenishment set the system back to the
1203 "normal" mode with differentiation left of path #3 in Fig. 9, producing layers of typical olivine
1204 gabbro with plagioclase enriched in An content, due to the elevated water contents in these
1205 melts.

1206
1207
1208

1209 **Table captions**

1210

1211 Table 1. Details of the experimental studies on hydrous MORB-type systems performed at
1212 shallow pressures used in this paper.

Table 1. Details of the experimental studies on hydrous MORB-type systems performed at shallow pressures used in this paper

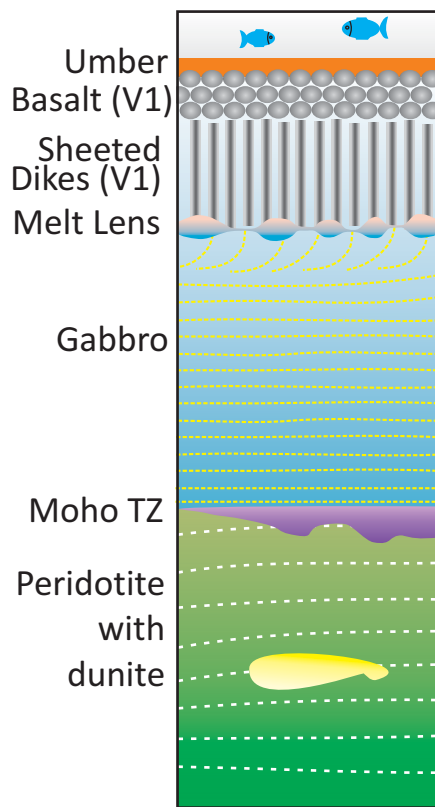
Study	System	Pressure	Temperature	Redox	Water addition	Water activity	Duration
Feig et al. (2006)	primitive MORB (natural system)	100, 200, 500 MPa	940 to 1220°C	QFM+1.0 to QFM+4.2	mixes of water and silver oxalate	0.04 - 1	22-91 hours
Feig et al. (2010)	primitive MORB (natural system)	200 MPa	940 to 1220°C	QFM-3.0 to QFM+2.1	mixes of water and silver oxalate	0.02 - 1	2-115 hours
Berndt et al. (2005)	model MORB	200 MPa	950 to 1150°C	QFM-3.4 to QFM+4.2	use of pre-hydrated glasses	0.02 - 1	2-72 hours
Koepke et al. (2018)	late-stage system (FeTi basalt)	200 MPa	850 to 1050°C	QFM-1.1 to QFM+3.2	mixes of water and silver oxalate	0.07 - 1	48-170 hours

Chemical compositions

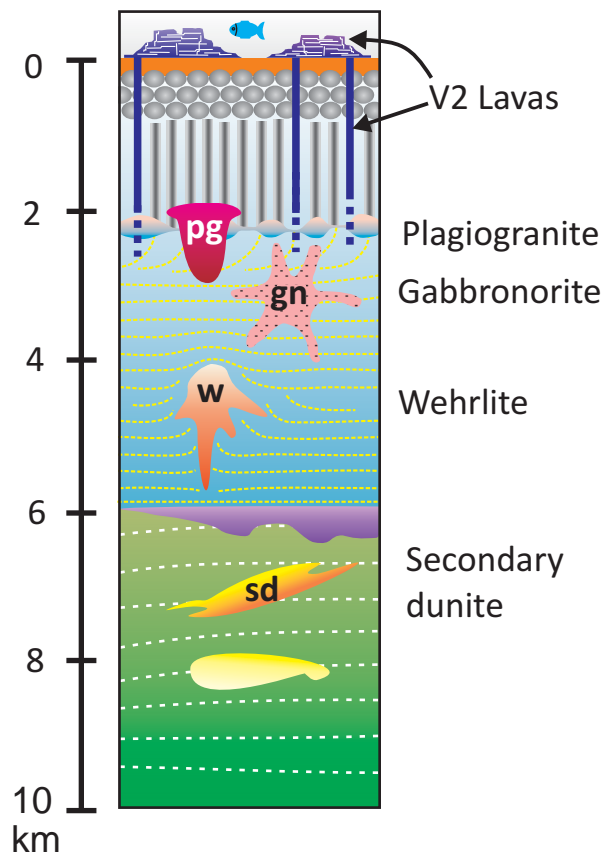
Study	SiO ₂	TiO ₂	Al ₂ O ₃	FeO _{tot}	MnO	MgO	CaO	Na ₂ O	K ₂ O	P ₂ O ₅	Total
Feig et al. (2006, 2010)	50.43	0.35	17.18	6.50	0.16	10.12	11.54	2.84	0.04	< 0.03	99.16
Berndt et al. (2005)	49.64	0.87	16.07	8.63	0.15	9.77	12.44	2.28	0.08	0.08	100.0
Koepke et al. (2018)	49.56	3.73	11.42	17.92	0.31	3.89	8.93	2.85	0.28	0.65	99.66

Koepke et al., Table 1

Phase 1: normal crust



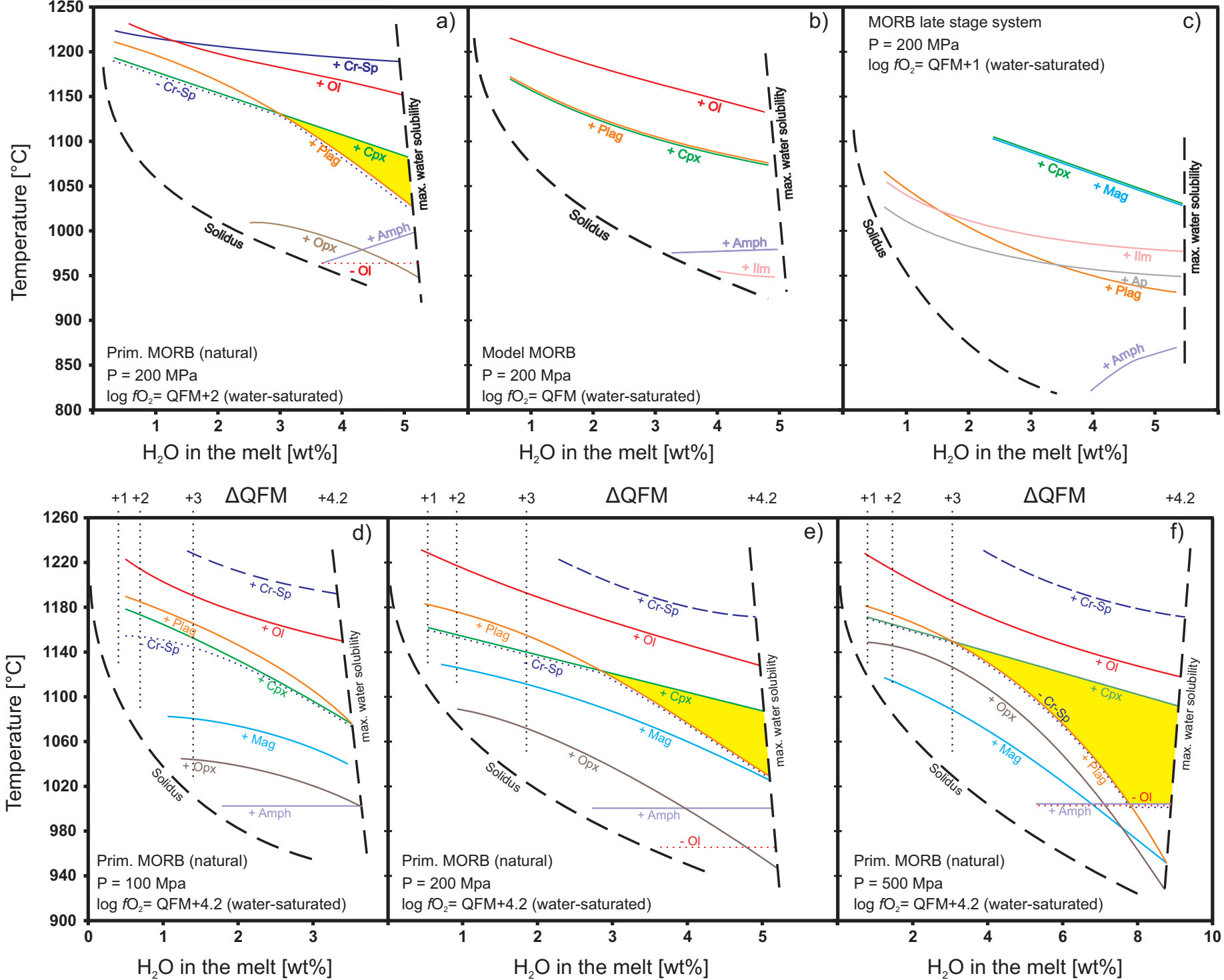
Phase 2: late stage lithologies



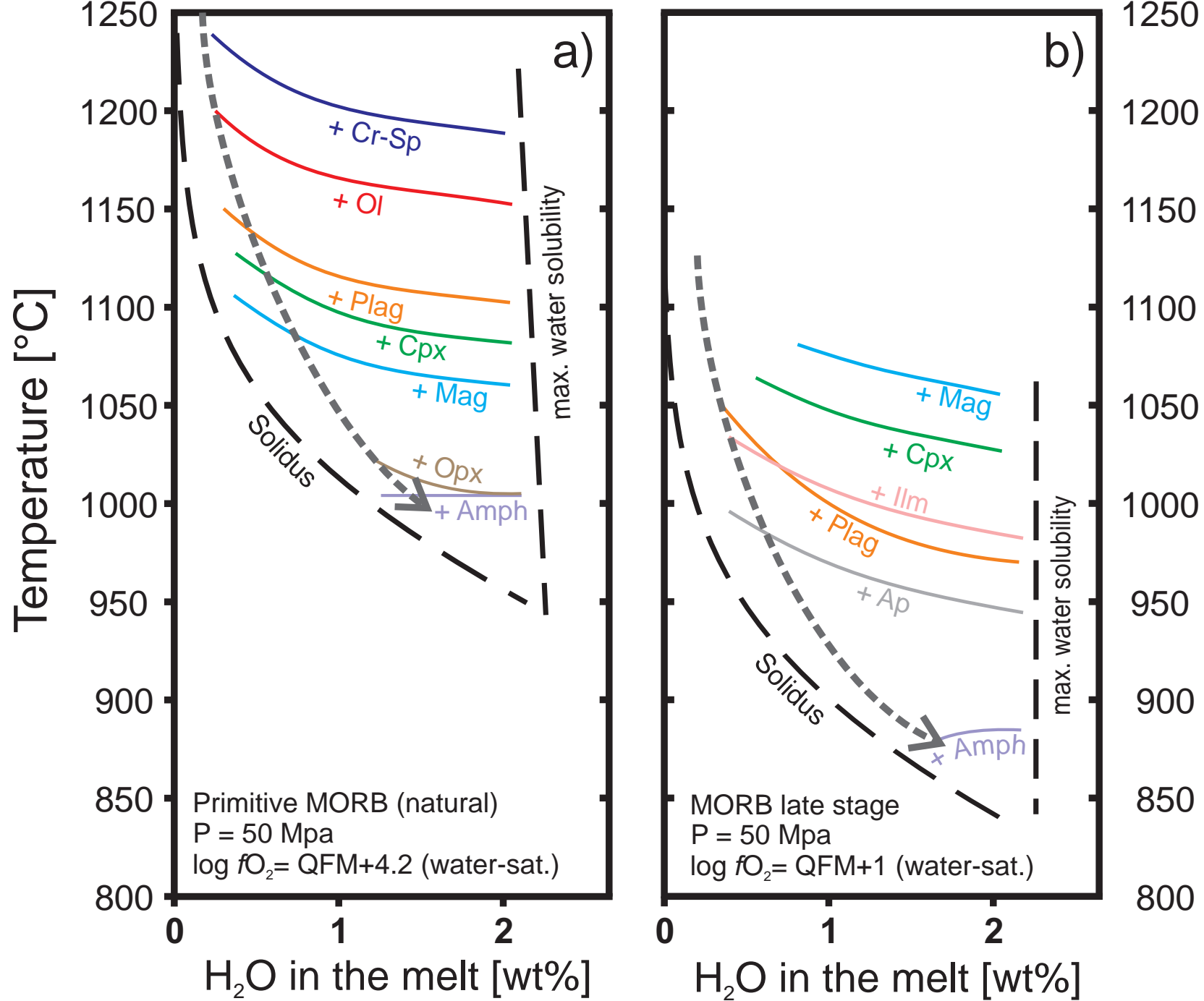
Koepke et al., Fig. 1



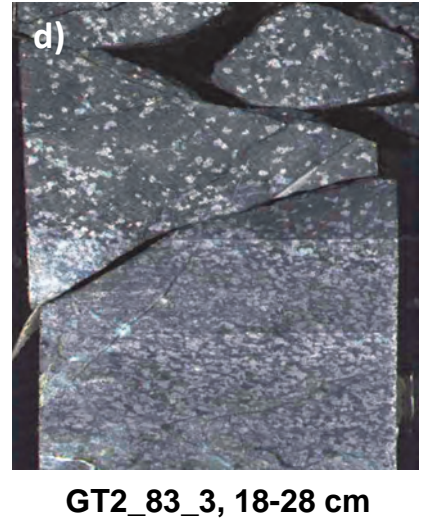
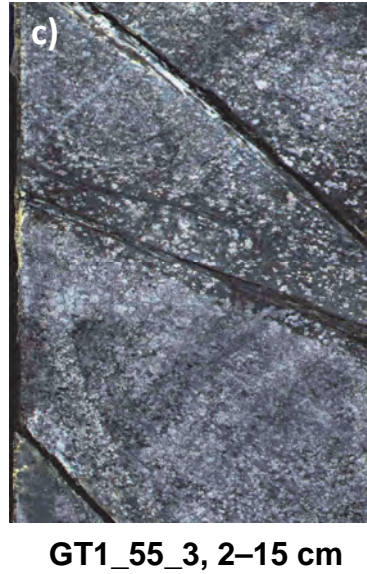
Koepke et al., Fig. 2



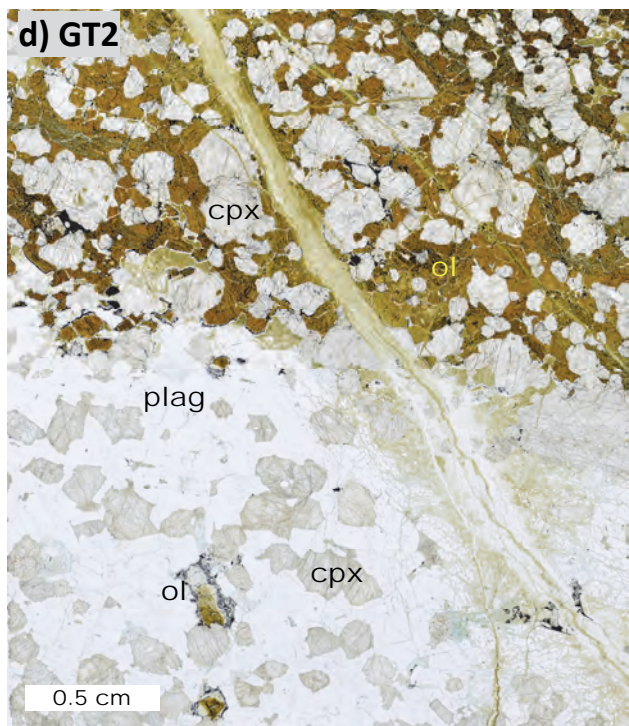
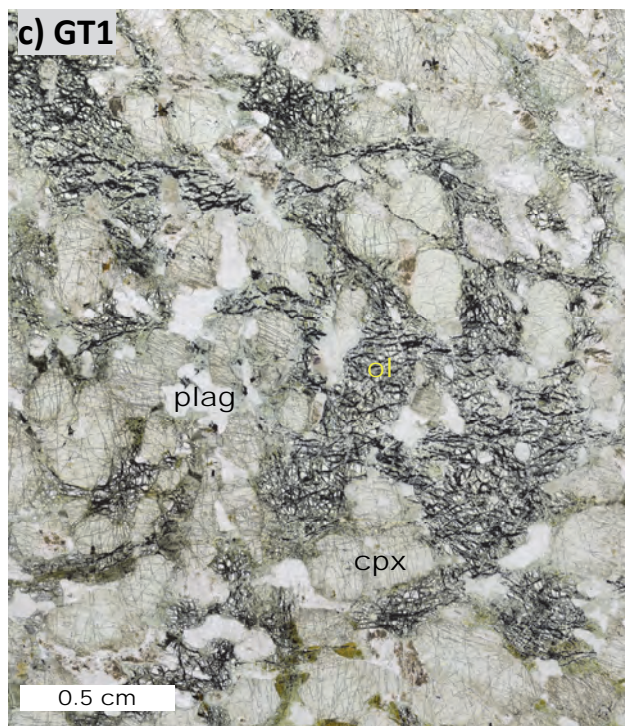
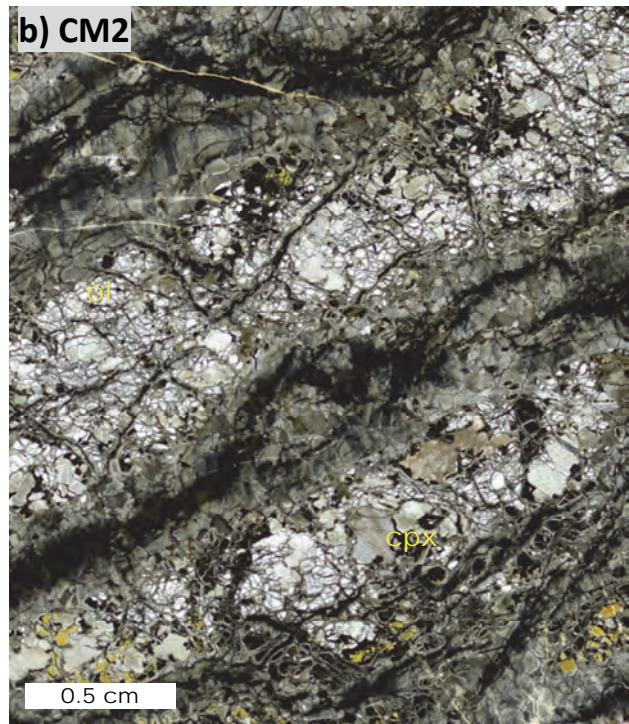
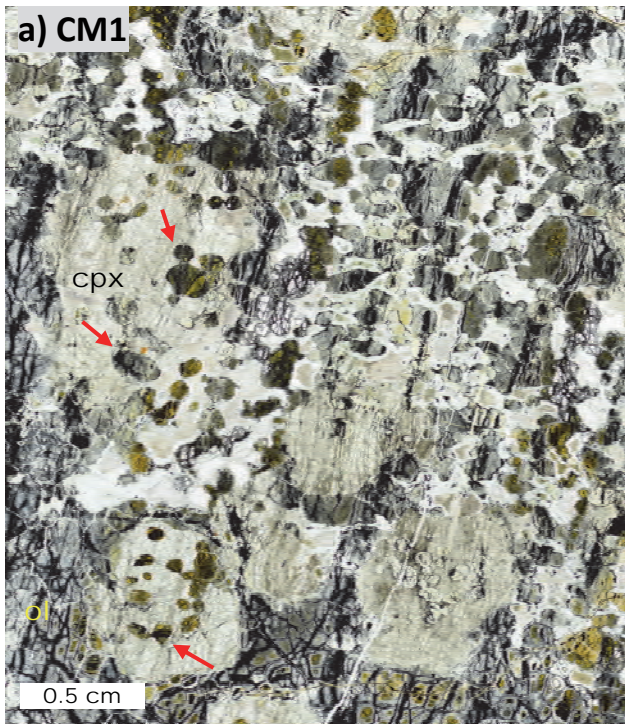
Koepke et al., Fig. 3



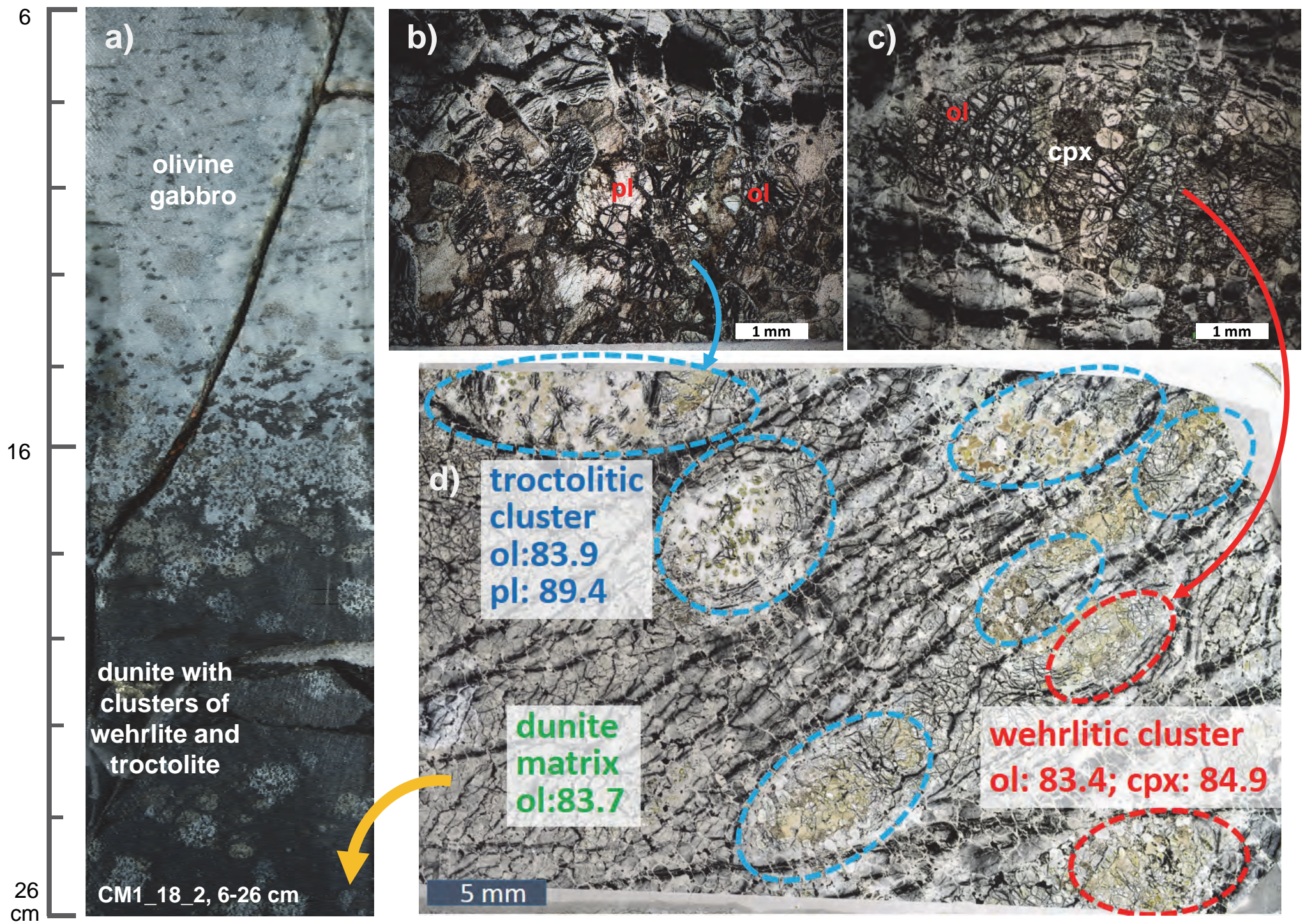
Koepke et al., Fig. 4



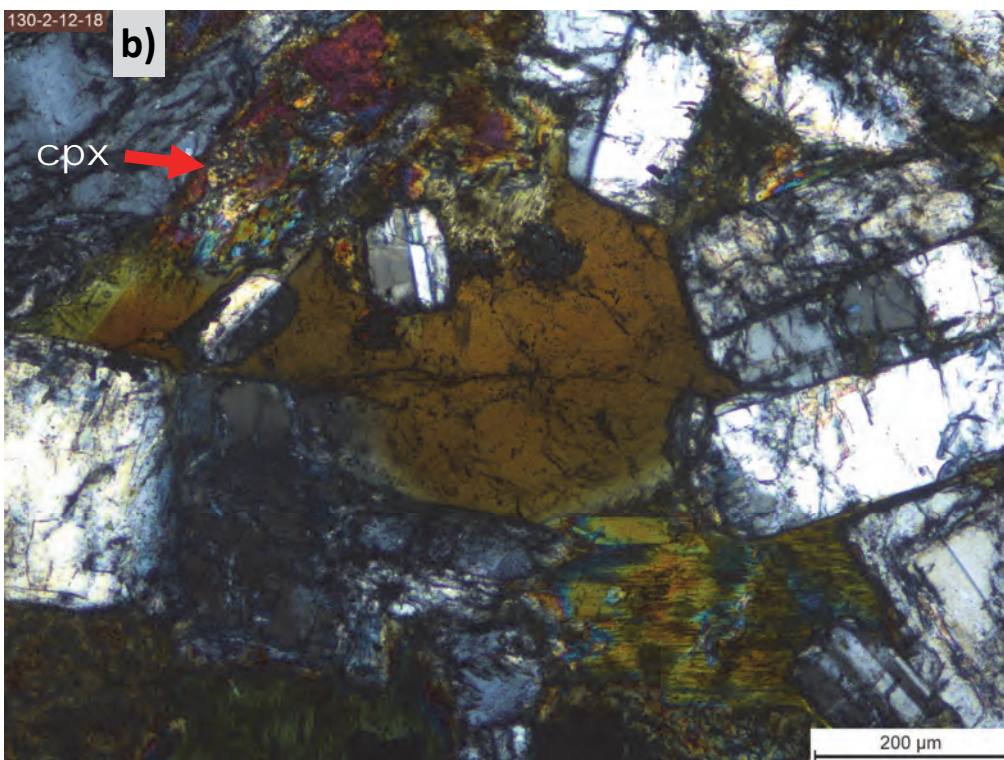
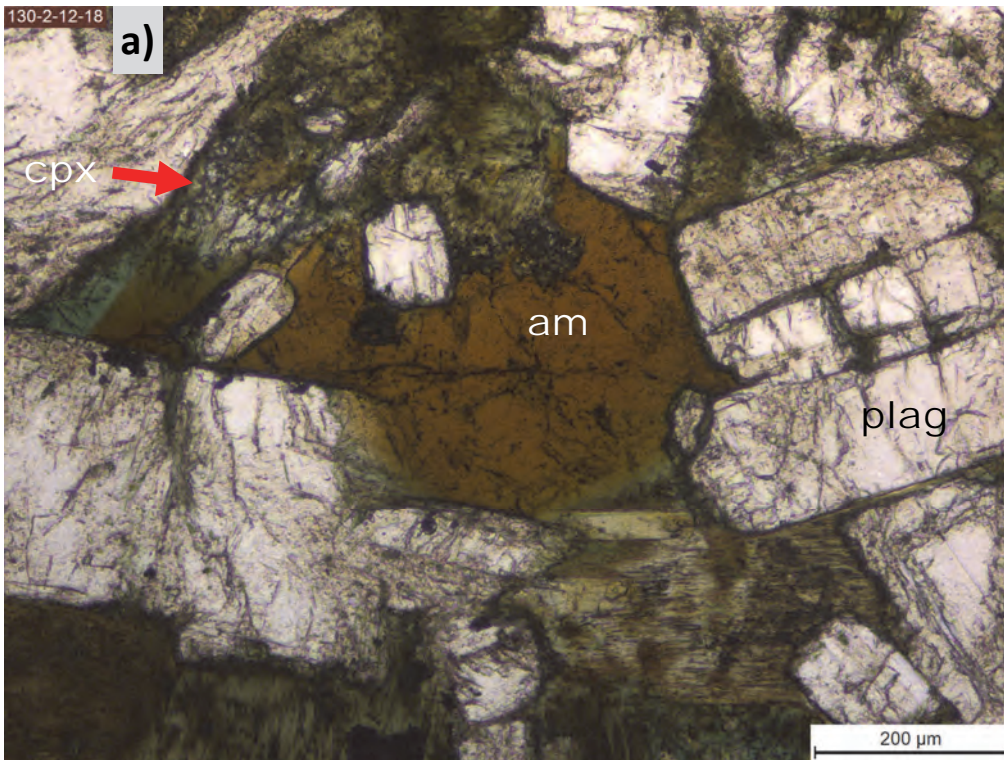
Koepke et al., Fig. 5



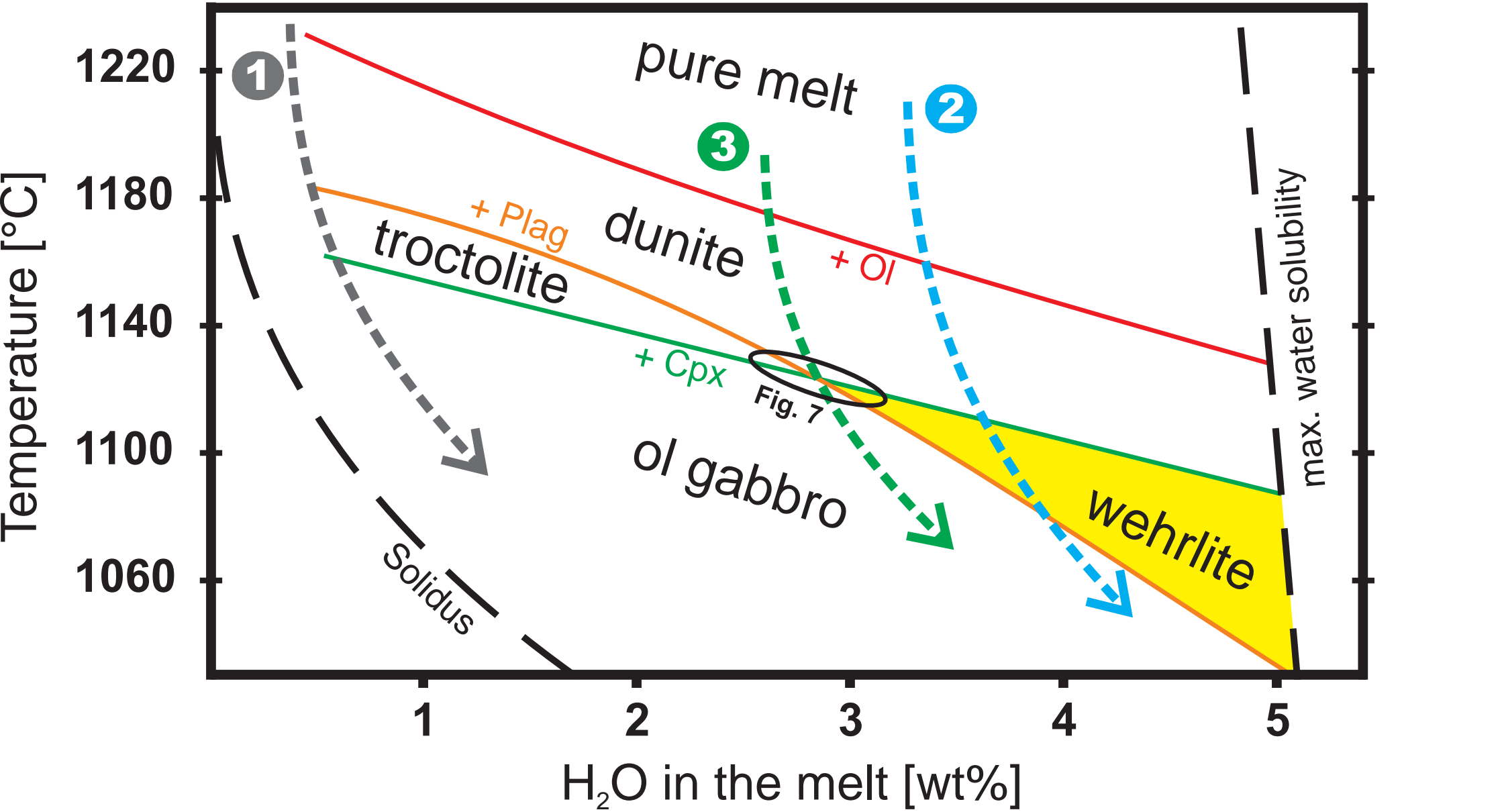
Koepke et al., Fig. 6



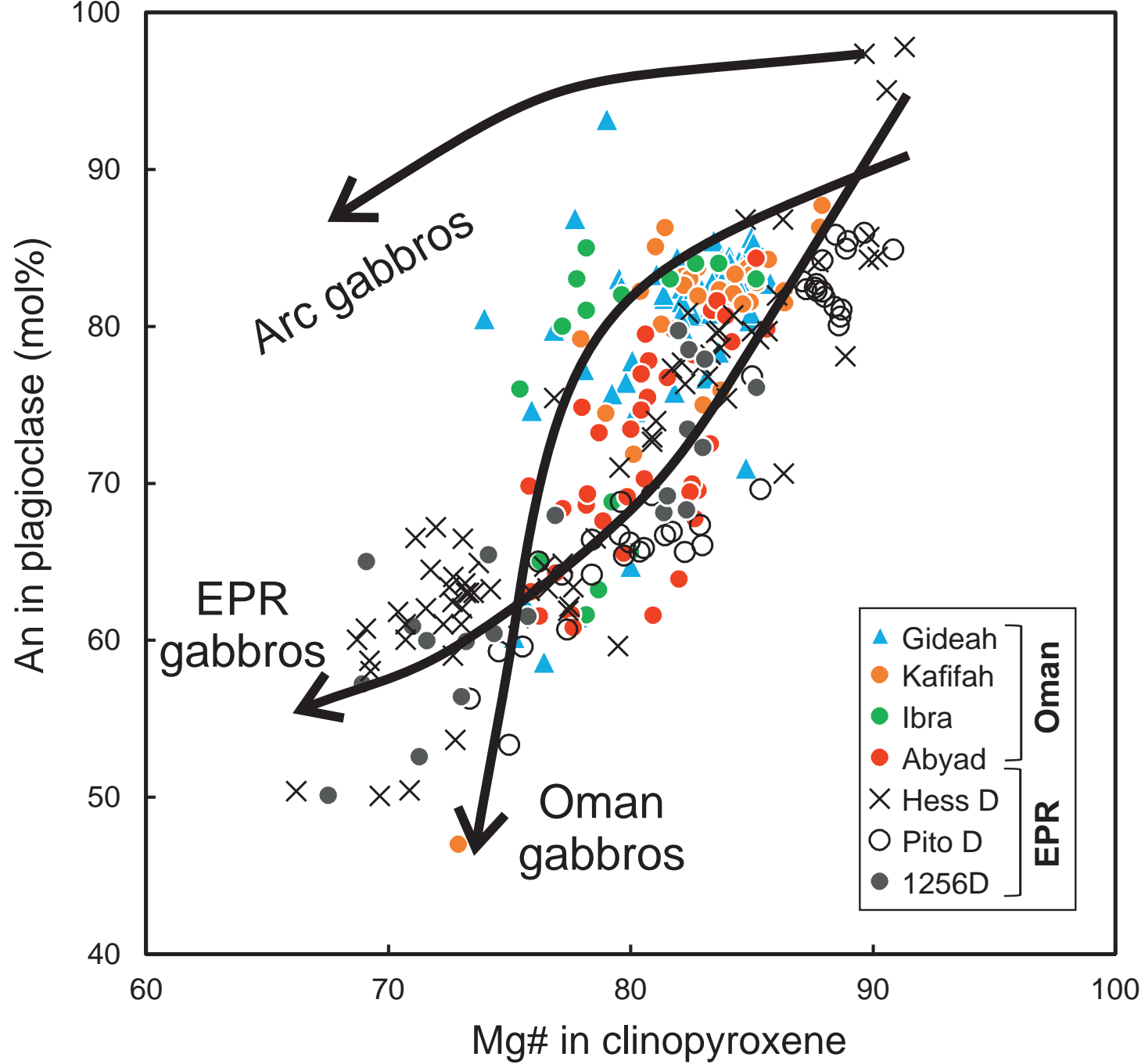
Koepke et al., Fig. 7



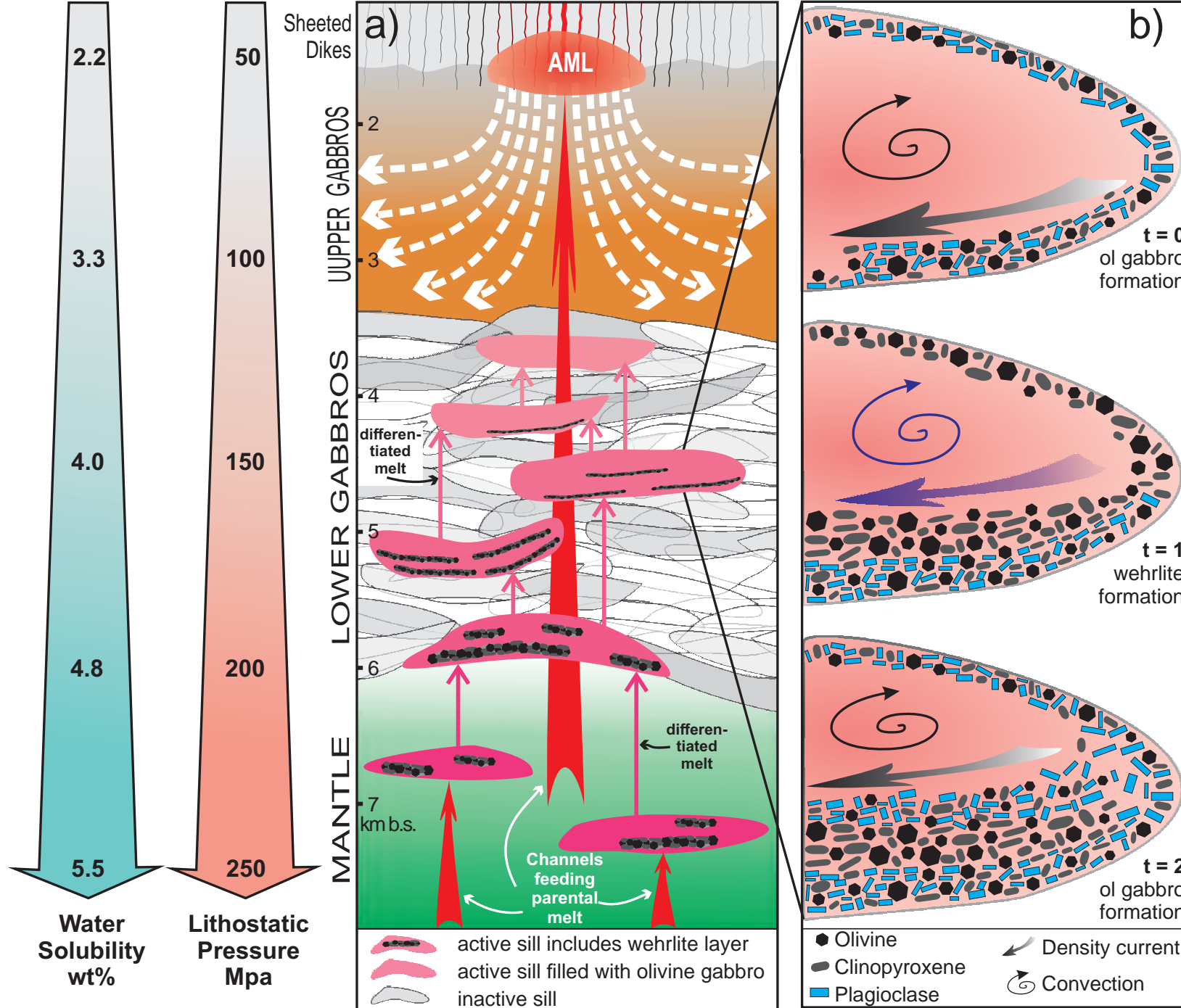
Koepke et al., Fig. 8



Koepke et al., Fig. 9



Koepke et al., Fig. 10



Koepke et al., Fig. 11